

# Workspace-Based Model Predictive Control for Cable-Driven Robots

Chen Song  and Darwin Lau , *Senior Member, IEEE*

**Abstract**—The control of cable-driven robots is challenging due to the system’s nonlinearity, actuation redundancy, and the unilaterally bounded actuation constraints. To solve this problem, a workspace-based model predictive control (W-MPC) scheme is proposed, which combines the online model predictive control with offline workspace analysis. Using the workspace, a set of convex constraints can be generated for a given reference trajectory. This can then be used to formulate a convex optimization problem for the online W-MPC. Meanwhile, strict recursive feasibility and stability are obtained by taking advantage of the predictive feature of MPC. To demonstrate the effectiveness of the proposed W-MPC, simulation was performed on a 2-link planar cable-driven robot and a spatial cable-driven parallel robot for both nominal and non-nominal scenarios. Hardware experiment was also carried out using a 3 degree-of-freedom planar cable robot. The results show that the controller is efficient and effective to perform motion tracking with the cable force constraints satisfied despite the existence of various model uncertainties.

**Index Terms**—Cable-driven robot, feedback linearization, model predictive control, workspace analysis.

## I. INTRODUCTION

CABLE-DRIVEN robots (CDRs) are systems that rely on cables to provide actuating forces. Compared with joint-driven robots, CDRs have significantly reduced weight and inertia. This results in a large potential workspace, and increased payload and speed capabilities, making it suitable for applications such as large-scale telescopes [1], motion simulation [2], heavy-lifting crane [3], building construction [4], and ultrafast manipulators [5]. Furthermore, multiple link CDRs are used as hyperredundant manipulators [6], musculoskeletal robots [7], and in rehabilitation [8].

While the cable actuation brings advantages for CDRs, one major limitation is that it can only provide bounded tensile forces (*unilateral actuation*). The lower bound on cable forces avoids cable slackness and the upper bound exists due to the maximum capabilities of actuators as well as to avoid cable breakage. These constraints on the cable forces create unique challenges in the

Manuscript received 5 June 2021; revised 30 September 2021; accepted 25 December 2021. Date of publication 2 February 2022; date of current version 8 August 2022. This work was supported by the Research Grants Council under Grant 24200516. This paper was recommended for publication by Associate Editor Q. Li and Editor E. Yoshida upon evaluation of the reviewers’ comments. (Corresponding author: Darwin Lau.)

The authors are with the Department of Mechanical and Automation Engineering, The Chinese University of Hong Kong, Hong Kong SAR 999077, China (e-mail: chensong@link.cuhk.edu.hk; darwinlau@cuhk.edu.hk).

Color versions of one or more figures in this article are available at <https://doi.org/10.1109/TRO.2021.3139585>.

Digital Object Identifier 10.1109/TRO.2021.3139585

analysis [9], [10] and control of CDRs compared with bilaterally actuated robots [11]. Moreover, CDRs are often redundantly actuated in order to be fully constrained. As a result, the control problem to solve for the cable forces to track desired motions is challenging due to the system nonlinearity, actuation constraints, and redundancy.

As it is difficult to simultaneously tackle these challenges, a *cascaded approach* comprising two sequential steps is commonly used in CDR control. First, the *joint control effort* is resolved assuming that the actuation is directly applied at the joints rather than through cables. This step handles the system nonlinearities, uncertainties, and disturbances, but not the actuation redundancy and constraints. Traditional joint space control methods, such as computed torque control (CTC) [12], [13], adaptive robust control [14], robust proportional–integral–derivative (PID) control [15], and sliding-mode control [16], can be directly used. The second step resolves the cable forces from the joint control effort using CDR *inverse dynamics* algorithms [17]–[19] to ensure that the constraints are satisfied with redundancy resolved.

Although the cascaded scheme is straightforward to implement, its primary drawback is the lack of guarantee such that the control effort generated from the first step can be executed by the inverse dynamics of the second step subject to cable force constraints (*feasibility*). One way to address this issue is to consider the cable force constraints in the control effort generation strategy, hence coupling the two cascaded steps. In [20], a CTC with an adjustable force lower bound was studied, but only offered very limited benefit in ensuring feasibility. In [21], a varying gain CTC was proposed, where the gains were solved through an optimization problem to ensure feasibility. However, the feasibility is achieved at the cost of lower tracking performance and possible instability.

The above works are all *reactive control* approaches where only the tracking error and constraints at the current time instance are considered. As a result, there is no guarantee on the feasibility of the future control steps (*recursive feasibility*). To address this, the use of reference governors [22], [23] was proposed for CDRs [24], [25], where the control reference (*setpoint*) of an unconstrained stabilizing *primal controller* is modified to guarantee the recursive feasibility. In practice, a fast feasible setpoint generation is essential to achieve reference tracking. However, the generation of feasible setpoint requires a large number of control input calculations and feasibility validations. As such, this approach has only been applied to specific types of CDRs, such as suspended CDRs with translation motion [24],

[25], where an analytical closed-form solution to the primal controller exists. Hence, it is difficult to apply this method to CDRs in general.

Given the CDR control requirements, including resolving actuation redundancy and offering recursive feasibility, model predictive control (MPC) [26], [27] is a highly suitable candidate solution. Using MPC, the cable forces can be solved through a constrained optimization problem to produce a desired tracking motion within a *finite horizon*. Due to the nonlinearity of the CDRs' equation of motion (EoM), the resulting nonlinear MPC (NMPC) will be a nonconvex optimization problem that is very difficult to solve. In [27], a black-box optimizer was used to tackle the nonconvexity, where the resulting NMPC cannot be used for real-time control given the huge computational load. In [28] and [29], a simplified MPC was applied on CDRs where a constant dynamics model is used throughout the horizon, resulting in a convex optimization problem. However, this simplification relies on the assumption of slow system dynamics, which is not always true.

Alternatively, in [26] a more systematic approach of approximating and solving the NMPC as a convex optimization problem was adopted, where the *convexification* is achieved by linearizing the EoM about the *linearization points* [30]. By selecting the linearization points from the reference trajectory, the linearized MPC is easily derived. Unfortunately, linearized MPC disallows large deviation from reference where large linearization error may occur, leading to instability or infeasibility [31]. To mitigate this problem, sequential quadratic programming (SQP) can be used to recursively solve the NMPC based on the latest trajectory prediction [32]. To lower the computational cost, real-time iteration MPC (RTI-MPC) [33] was also applied to CDR control [26], with only a single SQP iteration performed using the prediction from the previous control cycle. Nonetheless, the computational load is still high at each control cycle as multiple model linearizations and discretizations are required.

Feedback linearization (FL) is an alternative approach to convexify NMPC [34]. In FL, the *feedback linearizable* nonlinear system is converted into a linear time-invariant (LTI) system, using the associated *state diffeomorphism* and *nonlinear state feedback*. While FL is widely used in the unconstrained nonlinear control problems, its application in constrained control, such as MPC, is still limited mainly due to the reintroduction of nonlinearity in some inequality constraints, such as the input constraints, which often results in a nonconvex optimization problem. In order to restore convexity, various *constraint convexification* approaches have been proposed, including the *prediction based convexification* [35], [36] and the *reachable set-based convexification* [37], [38]. The former is generally easy to compute but lacks strict feasibility guarantee, especially when the actual trajectory deviates too much from the prediction, while the latter guarantees strict feasibility but is computationally prohibitive. Despite these, the combination of FL and MPC offers valuable insights into the convexification of the NMPC for CDRs.

In this article, a new *workspace-based MPC approach (W-MPC)* that uses CDR workspace to convexify the NMPC problem is proposed. First, the nonlinear system dynamics is converted to become LTI by selecting the joint acceleration as the

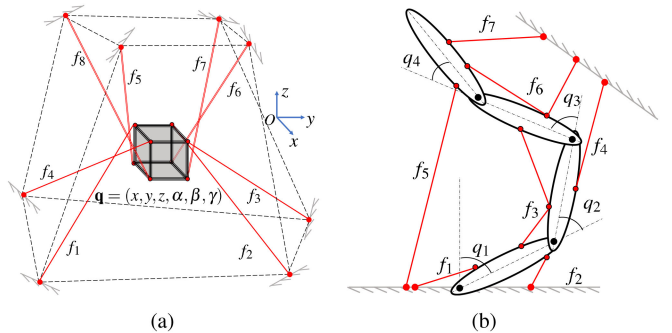


Fig. 1. Cable-driven robot models. (a) Spatial CDR example. (b) Multi-link CDR example.

*virtual control input*. To resolve the nonconvexity caused by the cable force constraints, workspace analysis is used to determine a set of box constraints on the CDR acceleration, velocity and pose such that the original input constraints can always be satisfied. Using the workspace-derived convex sets that are computed offline, it is shown that the NMPC can be transformed into a linear MPC that can be solved online using quadratic programming (QP). The stability and recursive feasibility of W-MPC are also proven. Using CASPR [39], simulations and hardware experiment on different CDRs show the characteristics and advantages of the proposed controller.

To the best of the authors' knowledge, this is the first MPC for robotic systems that uses workspace analysis in order to convexify the optimization problem. This approach brings four major advantages. First, recursive feasibility and stability are strictly guaranteed in nominal case with some *inherent robustness* in non-nominal cases. Second, the proposed approach is computationally efficient, requiring only one model evaluation and QP solving in each control cycle. In contrast, RTI-MPC needs to solve one QP and  $N$  (prediction horizon) model discretizations and linearizations. Third, different types of workspace can be incorporated, such as the interference-free workspace [40]. Finally, the proposed novel framework can be potentially applied on other types of robotic systems.

The remainder of the article is organized as follows. Section II introduces the required background. The W-MPC framework is proposed in Section III, followed by detailed derivation of the workspace for W-MPC in Section IV. The effectiveness of W-MPC is demonstrated through extensive simulations in Section V as well as hardware validation in Section VI. Based on the results, discussions on the performance and features of W-MPC are given in Section VII. Section VIII concludes this article. To offer theoretical completeness, proofs of stability and recursive feasibility of the proposed W-MPC are provided in Appendix A.

## II. BACKGROUND

### A. Cable-Driven Robot Model

CDRs are composed of a single or multiple rigid bodies, as illustrated in Fig. 1(a) and (b), respectively. The generalized EoM for any CDR with  $n$  degrees-of-freedom (DoFs) and  $m$

actuating cables can be given in the following form [41]:

$$M(\mathbf{q})\ddot{\mathbf{q}} + \mathbf{c}(\mathbf{q}, \dot{\mathbf{q}}) + \mathbf{g}(\mathbf{q}) = -L^\top(\mathbf{q})\mathbf{f} \quad (1)$$

where  $\mathbf{q} = [q_1, \dots, q_n]^\top \in \mathbb{R}^n$  is the generalized coordinate corresponding to the system DoFs and  $\mathbf{f} = [f_1, \dots, f_m]^\top \in \mathbb{R}^m$  is the cable force vector composed of forces on each actuating cables. The terms  $M \in \mathbb{R}^{n \times n}$ ,  $\mathbf{c} \in \mathbb{R}^n$  and  $\mathbf{g} \in \mathbb{R}^n$  are the inertia matrix, the centrifugal/Coriolis wrench, and the gravitational wrench, respectively. The Jacobian matrix  $L \in \mathbb{R}^{m \times n}$  defines the mapping between the cable and joint spaces. The cable force  $\mathbf{f}$  is confined by a lower bound  $\underline{\mathbf{f}}$  and an upper bound  $\bar{\mathbf{f}}$

$$\mathbf{f} \in \mathcal{F} := \{\mathbf{f} \in \mathbb{R}^m \mid \mathbf{0} \leq \mathbf{f} \leq \underline{\mathbf{f}} \leq \bar{\mathbf{f}}\}. \quad (2)$$

For CDR systems, the control input can be defined as the cable force vector  $\mathbf{u} = \mathbf{f}$ , and the state as  $\mathbf{x} = (\mathbf{q}, \dot{\mathbf{q}})$ , with the parentheses representing vector concatenation<sup>1</sup>. The CDR dynamics can then be described in the state space form

$$\dot{\mathbf{x}} = f(\mathbf{x}) + G(\mathbf{x})\mathbf{u} \quad (3)$$

$$\mathbf{u} \in \mathcal{F} \quad (4)$$

$$\mathbf{x} \in \mathcal{X} \quad (5)$$

$$f(\mathbf{x}) = \begin{bmatrix} \dot{\mathbf{q}} \\ -M^{-1}(\mathbf{q})[\mathbf{c}(\mathbf{q}, \dot{\mathbf{q}}) + \mathbf{g}(\mathbf{q})] \end{bmatrix}$$

$$G(\mathbf{x}) = \begin{bmatrix} 0_{n \times m} \\ -M^{-1}(\mathbf{q})L^\top(\mathbf{q}) \end{bmatrix}$$

with  $0_{n \times m}$  being an  $n$ -by- $m$  zero matrix. In general, the feasible state set  $\mathcal{X}$  is nonconvex and with no closed-form expression.

### B. Model Predictive Control for CDRs

MPC is a control method that optimizes the system behavior within a *finite horizon*. The MPC optimization problem involves several key components, including an *objective function*, constraints on the system dynamics (*EoM constraints*) and cable forces (*input constraints*), and *state constraints*. From a computational perspective, the system model should be discrete so that the number of optimizing variables is tractable. Considering a time interval  $\Delta t$ , the state at time step  $k$  (with the corresponding time  $t_k = k \cdot \Delta t$ ) can be expressed as  $\mathbf{x}_k = (\mathbf{q}_k, \dot{\mathbf{q}}_k)$ , where  $\mathbf{q}_k$  and  $\dot{\mathbf{q}}_k$  are the joint pose and velocity, respectively. The input  $\mathbf{u}_k$  corresponds to the cable force  $\mathbf{f}_k$  at time  $t_k$ . Then, the discretized version of (3) can be represented by

$$\mathbf{x}_{k+1} = F(\mathbf{x}_k, \mathbf{u}_k) \quad (6)$$

where  $F$  is in general a nonlinear function that needs to be numerically derived by solving the ordinary differential (3) for the time interval  $[t_k, t_k + \Delta t]$ . For the control task, the reference state that should be tracked by the controller at time step  $k$  is denoted as  $\mathbf{x}_k^r = (\mathbf{q}_k^r, \dot{\mathbf{q}}_k^r)$ .

<sup>1</sup>Vectors are column vectors by default and parentheses denote vertical concatenation:  $(\mathbf{q}, \dot{\mathbf{q}}) := [\mathbf{q}^\top, \dot{\mathbf{q}}^\top]^\top$ .

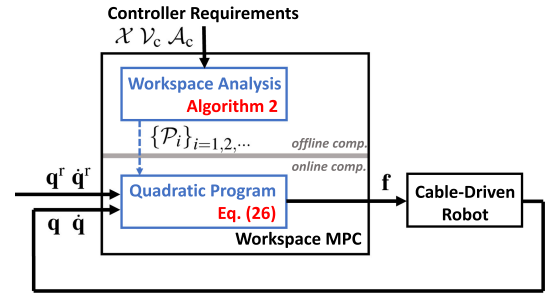


Fig. 2. Structure of the proposed workspace-based MPC ( $\mathcal{X}$ ,  $\mathcal{V}_c$ , and  $\mathcal{A}_c$  define the required state, joint velocity, and joint acceleration constraints while  $\mathcal{P}_i$  defines the derived joint pose constraints for a given reference trajectory).

For an  $N$  step horizon, the horizon prediction for state and control input at time step  $k$  are denoted as  $\mathbf{X}_k = (\mathbf{x}_{k+1|k}, \dots, \mathbf{x}_{k+N|k})$  and  $\mathbf{U}_k = (\mathbf{u}_{k|k}, \dots, \mathbf{u}_{k+N-1|k})$ , respectively, where  $\mathbf{x}_{j|k}$  and  $\mathbf{u}_{j|k}$  are the state and control input of time step  $j$  predicted at time step  $k$ , respectively. The state reference for the horizon at time step  $k$  is expressed by  $\mathbf{X}_k^r = (\mathbf{x}_{k+1}^r, \dots, \mathbf{x}_{k+N}^r)$ .

The goal of the MPC is to achieve a good tracking performance while satisfying constraints (3), (4), and (5), which can be formulated into the optimization problem

$$\underset{\mathbf{U}_k}{\text{minimize}} \quad \|\mathbf{X}_k - \mathbf{X}_k^r\|_Q^2 + \|\mathbf{U}_k - \mathbf{U}_k^r\|_R^2 \quad (7a)$$

$$\text{subject to} \quad \mathbf{X}_k = F_N(\mathbf{x}_k, \mathbf{U}_k) \quad (7b)$$

$$\mathbf{U}_k \in \mathcal{F}^N \quad (7c)$$

$$\mathbf{X}_k \in \mathcal{X}^N \quad (7d)$$

where  $\mathcal{F}^N$  and  $\mathcal{X}^N$  represent the Cartesian products of  $N$  constant sets  $\mathcal{F}$  and  $\mathcal{X}$ , respectively, and  $\mathbf{U}_k^r$  is the reference control input sequence and (7b) represents the discrete system dynamics over the horizon

$$\begin{bmatrix} \mathbf{x}_{k+1|k} \\ \mathbf{x}_{k+2|k} \\ \vdots \\ \mathbf{x}_{k+N|k} \end{bmatrix} = \begin{bmatrix} F(\mathbf{x}_k, \mathbf{u}_{k|k}) \\ F(\mathbf{x}_{k+1|k}, \mathbf{u}_{k+1|k}) \\ \vdots \\ F(\mathbf{x}_{k+N-1|k}, \mathbf{u}_{k+N-1|k}) \end{bmatrix} := F_N(\mathbf{x}_k, \mathbf{U}_k).$$

Problem (7) is classified as nonlinear MPC and is nonconvex due to the nonlinear equality constraint (7b).

## III. PROPOSED WORKSPACE-BASED MPC

The proposed W-MPC framework consists of two major components (Fig. 2): 1) *Online* MPC that generates the command cable forces by solving a quadratic program; and 2) *offline* workspace analysis to generate a set of convex constraints for the online MPC.

### A. FL-Inspired MPC for CDRs

A major difficulty in solving the NMPC problem (7) is caused by the nonlinear equality constraint (3). To work around this difficulty, an alternative MPC formulation, which is inspired by FL, can be derived with an LTI system dynamics being used. To

achieve this, a virtual input  $\mathbf{v}$  is selected as the joint acceleration  $\mathbf{v} = \ddot{\mathbf{q}}$ . Using (1), the *actuation mapping* from control input  $\mathbf{f}$  to virtual input  $\mathbf{v}$  is defined as

$$\mathbf{v} = \underbrace{[\mathbf{c}(\mathbf{q}, \dot{\mathbf{q}}) + \mathbf{g}(\mathbf{q})]}_{\mathbf{s}(\mathbf{x})} + \underbrace{[-\mathbf{M}^{-1}(\mathbf{q}) \mathbf{L}^\top(\mathbf{q})]}_{\mathbf{T}(\mathbf{x})} \mathbf{f}. \quad (8)$$

Assuming a constant virtual input within the control interval  $\Delta t$ , the dynamics becomes LTI, i.e., a *discrete double integrator*

$$\mathbf{x}_{k+1} = \underbrace{\begin{bmatrix} \mathbf{I}_{n \times n} & \Delta t \cdot \mathbf{I}_{n \times n} \\ 0_{n \times n} & \mathbf{I}_{n \times n} \end{bmatrix}}_{\mathbf{A}_d} \mathbf{x}_k + \underbrace{\begin{bmatrix} \frac{1}{2} \Delta t^2 \cdot \mathbf{I}_{n \times n} \\ \Delta t \cdot \mathbf{I}_{n \times n} \end{bmatrix}}_{\mathbf{B}_d} \mathbf{v}_k \quad (9)$$

where  $\mathbf{v}_k$  is the virtual input at time step  $k$ . As such, for a given initial state feedback  $\mathbf{x}_k$ , the state prediction  $\mathbf{X}_k$  and the virtual input prediction  $\mathbf{V}_k = (\mathbf{v}_{k|k}, \dots, \mathbf{v}_{k+N-1|k})$  satisfy

$$\mathbf{X}_k = \underbrace{\begin{bmatrix} \mathbf{A}_d \\ \mathbf{A}_d^2 \\ \vdots \\ \mathbf{A}_d^N \end{bmatrix}}_A \mathbf{x}_k + \underbrace{\begin{bmatrix} \mathbf{B}_d & 0 & \cdots & 0 \\ \mathbf{A}_d \mathbf{B}_d & \mathbf{B}_d & \cdots & 0 \\ \vdots & \vdots & \ddots & \vdots \\ \mathbf{A}_d^{N-1} \mathbf{B}_d & \mathbf{A}_d^{N-2} \mathbf{B}_d & \cdots & \mathbf{B}_d \end{bmatrix}}_B \mathbf{V}_k. \quad (10)$$

Considering the actuation mapping (8), the cable force constraint (2) becomes a constraint on the virtual input  $\mathbf{v} \in \mathcal{A}(\mathbf{x})$ , where  $\mathcal{A}(\mathbf{x})$  is defined as the *virtual input constraint set*

$$\mathcal{A}(\mathbf{x}) = \{\mathbf{v} \in \mathbb{R}^n \mid \mathbf{v} = \mathbf{s}(\mathbf{x}) + \mathbf{T}(\mathbf{x}) \mathbf{f}, \exists \mathbf{f} \in \mathcal{F}\}. \quad (11)$$

As such, the virtual input constraints over the entire horizon at time step  $k$  can be expressed as

$$\mathbf{V}_k \in \underbrace{\mathcal{A}(\mathbf{x}_k) \times \cdots \times \mathcal{A}(\mathbf{x}_{k+N-1|k})}_{:= \mathcal{A}_N(\mathbf{x}_k, \mathbf{V}_k)}. \quad (12)$$

Since by definition  $\mathcal{A}_N(\mathbf{x}_k, \mathbf{V}_k)$  is nonlinearly dependent on the virtual input horizon  $\mathbf{V}_k$ , the constraint  $\mathbf{V}_k \in \mathcal{A}_N(\mathbf{x}_k, \mathbf{V}_k)$  is generally nonconvex. Finally, similar to the objective function (7a) and the constraints (10), (12), and (7d), the FL-inspired MPC (FLIMPC) can be formulated as

$$\begin{aligned} & \underset{\mathbf{V}_k}{\text{minimize}} \quad \|\mathbf{X}_k - \mathbf{X}_k^r\|_Q^2 + \|\mathbf{V}_k - \mathbf{V}_k^r\|_R^2 \\ & \text{subject to} \quad \mathbf{X}_k = \mathbf{A}\mathbf{x}_k + \mathbf{B}\mathbf{V}_k \\ & \quad \mathbf{V}_k \in \mathcal{A}_N(\mathbf{x}_k, \mathbf{V}_k) \\ & \quad \mathbf{X}_k \in \mathcal{X}^N \end{aligned} \quad (13)$$

where  $\mathbf{V}_k^r = (\ddot{\mathbf{q}}_k^r, \dots, \ddot{\mathbf{q}}_{k+N-1}^r)$  is the reference virtual input for the horizon.

Although both the optimization problems (7) and (13) are *nonconvex*, the nonconvexity for the NMPC (7) is due to the nonlinear equality constraint, while for the FLIMPC (13), it comes from the nonconvex virtual input set constraints. It will be shown that the set constraint of FLIMPC can be easily convexified using the workspace of the CDR.

## B. Precomputed Workspace-Based MPC Convexification

Since the horizon virtual input constraint (12) is nonconvex and the feasible state set  $\mathcal{X}$  is potentially nonconvex, the convexification process begins with replacing the sets  $\mathcal{A}_N(\mathbf{x}_k, \mathbf{V}_k)$  and  $\mathcal{X}^N$  in (13) with convex sets where

$$\begin{aligned} \mathbf{X}_k &= \mathbf{A}\mathbf{x}_k + \mathbf{B}\mathbf{V}_k \\ \mathbf{V}_k &\in \mathcal{A}_k \times \cdots \times \mathcal{A}_{k+N-1} \\ \mathbf{X}_k &\in \mathcal{X}_{k+1} \times \cdots \times \mathcal{X}_{k+N}. \end{aligned} \quad (14)$$

With sets  $\mathcal{A}_i$ ,  $\mathcal{X}_{i+1}$ ,  $i = k, \dots, k+N-1$  being convex, the constraints in (14) are convex. In particular, for a given  $\mathbf{x}_k$ , the feasible set for  $\mathbf{v}_{k|k}$  can be defined using (11) as

$$\mathcal{A}_k = \{\mathbf{v}_k \in \mathbb{R}^n \mid \mathbf{M}_k \mathbf{v}_k + \mathbf{c}_k + \mathbf{g}_k = -\mathbf{L}_k^\top \mathbf{f}_k, \mathbf{f}_k \in \mathcal{F}\} \quad (15)$$

where  $\mathbf{M}_k = \mathbf{M}(\mathbf{q}_k)$ ,  $\mathbf{c}_k = \mathbf{c}(\mathbf{q}_k, \dot{\mathbf{q}}_k)$ ,  $\mathbf{g}_k = \mathbf{g}(\mathbf{q}_k)$ , and  $\mathbf{L}_k = \mathbf{L}(\mathbf{q}_k)$ .

However, the convex sets in (14) cannot be arbitrarily chosen, as they need to be strictly feasible, i.e., all the accelerations in these sets can be feasibly generated using the available cable forces (2), to ensure convexification validity. This inevitably makes the feasible region defined by (14) a subset of that in (13), such that the convexified constraints are conservative, which may result in poor control performance or even infeasibility. To address this, Conditions 1, 2, and 3 are proposed for the convexified constraint design.

*Condition 1 (Solution Safety):* Solutions feasible to the *convexified constraints* must also satisfy the *original constraints* from (13), i.e., for  $i = k, \dots, k+N-1$ , and  $\mathcal{X}_k = \{\mathbf{x}_k\}$ , the following holds:

$$\mathcal{X}_{i+1} \subset \mathcal{X} \quad (16a)$$

$$\forall \mathbf{x} \in \mathcal{X}_i : \mathcal{A}_i \subset \mathcal{A}(\mathbf{x}). \quad (16b)$$

*Condition 2 (Control Feasibility):* For a given state feedback  $\mathbf{x}_k$  that is close enough to the reference value  $\mathbf{x}_k^r$ , the solution set for the *convexified constraints* shall be nonempty.

*Condition 3 (Control Stability):* For a starting state  $\mathbf{x}_k$  that is close enough to the reference value  $\mathbf{x}_k^r$ , it is possible to find a stabilizing control law satisfying the *convexified constraints*.

The design of the convex sets from (14) to satisfy conditions 1, 2, and 3 is generally intractable. First, the design of the state constraint sets  $\mathcal{X}_{i+1}$  and virtual input constraint sets  $\mathcal{A}_i$  are coupled, see (16), hence requiring an iterative approach. Second, the convexification needs to be performed online for the specific feedback  $\mathbf{x}_k$ . Third, Condition 3 requires the consideration of potential control performance of the *convexified MPC* in the convexification set design.

To address the challenges in designing the convex sets in (14), the following simplifications can be made.

- 1) The virtual input constraint sets  $\mathcal{A}_i$ ,  $i \geq k+1$  are identical convex sets  $\mathcal{A}_c$ , i.e.,  $\mathcal{A}_i = \mathcal{A}_c$ ,  $i \geq k+1$ .
- 2) The sets  $\mathcal{X}_i$ , where  $(\mathbf{q}_i, \dot{\mathbf{q}}_i) \in \mathcal{X}_i$ , will be considered as the Cartesian product of two subspace convex sets  $\mathcal{P}_i$  and  $\mathcal{V}_c$ , where  $\mathbf{q}_i \in \mathcal{P}_i$ ,  $\dot{\mathbf{q}}_i \in \mathcal{V}_c$ , and  $\mathcal{X}_i = \mathcal{P}_i \times \mathcal{V}_c \subset \mathcal{X}$ .

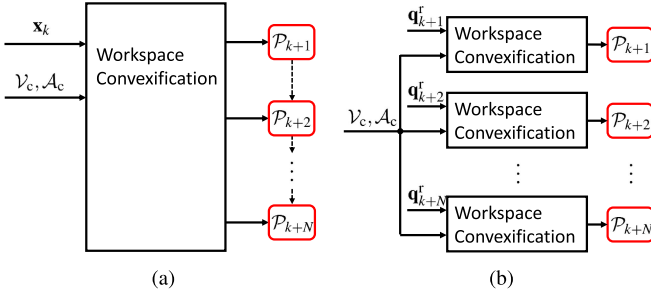


Fig. 3. Workspace-based convexification. (a) Online convexification. (b) Offline convexification.

As such

$$\mathbf{q}_i \in \mathcal{P}_i, \dot{\mathbf{q}}_i \in \mathcal{V}_c \Rightarrow (\mathbf{q}_i, \dot{\mathbf{q}}_i) \in \mathcal{X}. \quad (17)$$

It should be noted that both  $\mathcal{V}_c$  and  $\mathcal{A}_c$  shall be designed by the user to represent the allowed motion capability in the prediction horizon of MPC, while the pose sets  $\mathcal{P}_i$  can be subsequently derived using the workspace. Based on these simplifications, the convexified constraints in (14) can be expressed as

$$\begin{aligned} \mathbf{X}_k &= \mathbf{A}\mathbf{x}_k + \mathbf{B}\mathbf{V}_k \\ \mathbf{V}_k &\in \mathcal{A}_k \times \mathcal{A}_c^{N-1} \\ \mathbf{X}_k &\in \mathcal{P}_{k+1} \times \mathcal{V}_c \times \cdots \times \mathcal{P}_{k+N} \times \mathcal{V}_c. \end{aligned} \quad (18)$$

Similar to conditions (16a) to (16b), the following conditions must be satisfied for the design of the convex sets  $\mathcal{A}_c$ ,  $\mathcal{V}_c$ , and  $\mathcal{P}_i$ , where  $i = k+1, \dots, k+N$  in (18)

$$\mathcal{P}_i \times \mathcal{V}_c \subset \mathcal{X} \quad (19a)$$

$$\forall \mathbf{x} \in \mathcal{P}_i \times \mathcal{V}_c : \mathcal{A}_c \subset \mathcal{A}(\mathbf{x}). \quad (19b)$$

In fact, a largest set  $\mathcal{P}$  exists satisfying

$$\mathcal{P} \times \mathcal{V}_c \subset \mathcal{X} \quad (20a)$$

$$\forall \mathbf{x} \in \mathcal{P} \times \mathcal{V}_c : \mathcal{A}_c \subset \mathcal{A}(\mathbf{x}). \quad (20b)$$

Set  $\mathcal{P}$  is effectively a workspace (*the W-MPC workspace*) which will be discussed more detailedly in Section IV. The problem of deriving the convexified constraints (19) becomes properly selecting a series of subsets of the W-MPC workspace

$$\mathcal{P}_i \subset \mathcal{P}. \quad (21)$$

Principally, the above pose sets  $\mathcal{P}_i$ ,  $i = k+1, \dots, k+N$  shall be dependent of each other as well as the state feedback  $\mathbf{x}_k$ . More specifically, consider the initial state set as  $\mathcal{X}_k = \{\mathbf{x}_k\}$  and the future state sets as  $\mathcal{X}_i = \mathcal{P}_i \times \mathcal{V}_c$ ,  $i = k+1, \dots, k+N$ ,  $\mathcal{X}_i$  shall be within the *reachable set* [42] of  $\mathcal{X}_{i-1}$  considering the linear system (9) and available virtual input set  $\mathcal{A}_c$ . The convexification process is illustrated in Fig. 3(a).

However, due to the extensive set operations involved in deriving the reachable sets and the lack of a closed-form representation of W-MPC workspace  $\mathcal{P}$ , the computational load to compute  $\mathcal{P}_i$ ,  $i = k+1, \dots, k+N$  is usually too large for online implementation. To resolve this problem, the concept of the *feasible pose corridor* is proposed for the W-MPC, which is composed of a series of interconnected hyperrectangles, as

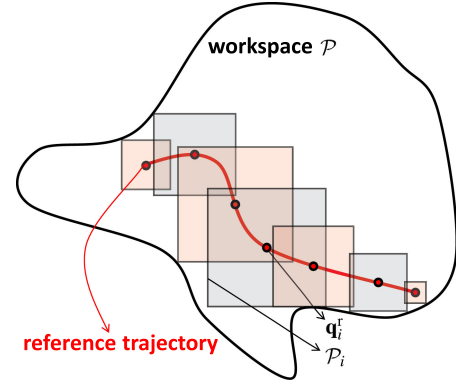


Fig. 4. Feasible pose corridor.

defined in Definition 2 and illustrated in Fig. 4. Since each hyperrectangle in the feasible pose corridor is a maximum workspace hyperrectangle, see Definition 1, centered at the reference point of a certain time step, the adjacent hyperrectangles will largely overlap.

**Definition 1 (Maximum Workspace Hyperrectangle):** For a pose  $\mathbf{q}$ , the maximum workspace hyperrectangle  $\mathcal{C}(\mathbf{q})$  is the largest hyperrectangle inside workspace  $\mathcal{P}$  centred at  $\mathbf{q}$ .

**Definition 2 (Feasible Pose Corridor):** The feasible pose corridor for a reference pose trajectory  $\mathbf{q}_i^r$ ,  $\forall i \in \mathcal{I}$ <sup>2</sup> refers to the set of maximum hyperrectangles  $\mathcal{P}_i$  corresponding to each reference pose  $\mathbf{q}_i^r$  for a given workspace  $\mathcal{P}$ . Fig. 4 illustrates the concept of the feasible pose corridor.

Finally, with the feasible pose corridor being used, Condition 4 states the requirements in the design of the sets  $\mathcal{V}_c$  and  $\mathcal{A}_c$  to ensure Conditions 1 to 3 (Theorem 1). It should be noted that the larger the margins in Condition 4 are, the larger deviation is allowed from reference according to Theorem 1, indicating a better robustness of the closed-loop system. Additionally, in Remark 1, a candidate design procedure to guarantee Condition 4 is introduced.

**Condition 4 (Reference Trajectory Safety):** Consider a reference trajectory  $\mathbf{q}_i^r, \dot{\mathbf{q}}_i^r, \ddot{\mathbf{q}}_i^r$ ,  $i \in \mathcal{I}$ , constant sets  $\mathcal{V}_c$  and  $\mathcal{A}_c$ , and a corresponding feasible pose corridor  $\mathcal{P}_i$ . Positive safety margins  $p, v, a$  shall exist such that  $(\tilde{\mathbf{q}}_i := \mathbf{q}_i - \mathbf{q}_i^r)$

$$\begin{aligned} \|\tilde{\mathbf{q}}_i\|_\infty &\leq p, \|\dot{\tilde{\mathbf{q}}}_i\|_\infty \leq v, \|\ddot{\tilde{\mathbf{q}}}_i\|_\infty \leq a \Rightarrow (\mathbf{q}_i, \dot{\mathbf{q}}_i, \ddot{\mathbf{q}}_i) \\ &\in \mathcal{P}_i \times \mathcal{V}_c \times \mathcal{A}_c \end{aligned}$$

i.e., the reference trajectory  $\mathbf{q}_i^r, \dot{\mathbf{q}}_i^r, \ddot{\mathbf{q}}_i^r$  stays inside of  $\mathcal{P}_i \times \mathcal{V}_c \times \mathcal{A}_c$  with non-zero distance to its boundaries.

**Theorem 1 (Workspace-Based Convexification):** Let the convexified constraints take the form of (18) with the pose sets selected as the maximum hyperrectangles from the feasible pose corridor. Given that Condition 4 is satisfied, there exists a neighborhood  $\|\mathbf{x}_k - \mathbf{x}_k^r\|_\infty \leq \epsilon$  with  $\epsilon > 0$  for the initial state  $\mathbf{x}_k$  such that Conditions 1–3 are satisfied.

*Proof:* Conditions 1–3 will be discussed separately.

<sup>2</sup>Set  $\mathcal{I}$  is a finite integer set  $\{1, 2, \dots, M\}$  with  $M$  representing the maximum time step index for a certain reference trajectory.

*Condition 1:* Since  $\mathcal{P}_i$  is designed to be a subset of the workspace  $\mathcal{P}$ , (21) and (20) are satisfied, which leads to

$$\begin{aligned} \mathcal{P}_i \times \mathcal{V}_c &\subset \mathcal{P} \times \mathcal{V}_c \subset \mathcal{X} \\ \forall \mathbf{x} \in \mathcal{P}_i \times \mathcal{V}_c &\subset \mathcal{P} \times \mathcal{V}_c : \mathcal{A}_c \subset \mathcal{A}(\mathbf{x}). \end{aligned}$$

Hence, by setting  $\mathcal{V}_i = \mathcal{V}_c$  and  $\mathcal{A}_i = \mathcal{A}_c$ , Condition 1 is satisfied.

*Condition 2:* For state within the local neighborhood  $\|\mathbf{x}_k - \mathbf{x}_k^r\|_\infty \leq \epsilon$ , it can be expressed as  $\mathbf{x}_k = \mathbf{x}_k^r + \tilde{\mathbf{x}}_k$ , where  $\|\tilde{\mathbf{x}}_k\|_\infty \leq \epsilon$ . Assuming  $\mathbf{V}_k = \mathbf{V}_k^r \in \mathcal{A}_k \times \mathcal{A}_c^{N-1}$ , the predicted state error over the horizon becomes

$$\mathbf{X}_k - \mathbf{X}_k^r = A(\mathbf{x}_k^r + \tilde{\mathbf{x}}_k) + B\mathbf{V}_k^r - \mathbf{X}_k^r = A\tilde{\mathbf{x}}_k.$$

From (9) and (10),  $\|A\|_\infty = 1 + N\Delta t$ , hence

$$\|\mathbf{X}_k - \mathbf{X}_k^r\|_\infty \leq \|A\|_\infty \|\tilde{\mathbf{x}}_k\|_\infty \leq (1 + N\Delta t)\epsilon.$$

As a result,  $\mathbf{X}_k \in \mathcal{P}_{k+1} \times \mathcal{V}_c \times \cdots \times \mathcal{P}_{k+N} \times \mathcal{V}_c$  hold for a small  $\epsilon$  under Condition 4, which guarantees Condition 2 to hold.

*Condition 3:* Consider a linear quadratic regulator (LQR) control gain  $K$  which defines a control law  $\tilde{\mathbf{v}}_k = -K \cdot \tilde{\mathbf{x}}_k$  that guarantees the infinite-horizon optimality [43]. Design

$$\mathbf{V}_k = \mathbf{V}_k^r + \tilde{\mathbf{V}}_k = \mathbf{V}_k^r + (-K\tilde{\mathbf{x}}_k, \mathbf{0}, \dots, \mathbf{0}) \quad (22)$$

then, the predicted horizon state error becomes

$$\begin{aligned} \mathbf{X}_k - \mathbf{X}_k^r &= A(\mathbf{x}_k^r + \tilde{\mathbf{x}}_k) + B(\mathbf{V}_k^r + \tilde{\mathbf{V}}_k) - \mathbf{X}_k^r \\ &= A\tilde{\mathbf{x}}_k - B_1 K \tilde{\mathbf{x}}_k = (A - B_1 K) \tilde{\mathbf{x}}_k \end{aligned}$$

where  $B_1 = [(B_d)^T (A_d B_d)^T \cdots (A_d^{N-1} B_d)^T]^T$ .

Since all the elements of the LQR control gain  $K$  are finite,  $\exists \eta, \xi > 0 : \| -K \|_\infty \leq \eta, \| A - B_1 K \|_\infty \leq \xi$ . Consequently,  $\|\mathbf{V}_k - \mathbf{V}_k^r\|_\infty = \| -K\Delta\mathbf{x}_k \|_\infty \leq \eta \cdot \epsilon$  and  $\|\mathbf{X}_k - \mathbf{X}_k^r\|_\infty \leq \xi \cdot \epsilon$ , guaranteeing  $\mathbf{V}_k \in \mathcal{A}_k \times \mathcal{A}_c^{N-1}$  and  $\mathbf{X}_k \in \mathcal{P}_{k+1} \times \mathcal{V}_c \times \cdots \times \mathcal{P}_{k+N} \times \mathcal{V}_c$  to hold for a small  $\epsilon$  if Condition 4 is satisfied. As a result, (22) represents a feasible solution to the convexified constraints (18), and the existence of the optimal control law  $\mathbf{v}_k = \mathbf{v}_k^r - K(\mathbf{x}_k - \mathbf{x}_k^r)$  proves Condition 3. ■

*Remark 1:* To guarantee Condition 4, both the reference trajectory and the sets  $\mathcal{V}_c$  and  $\mathcal{A}_c$  need to be carefully designed, for which the following procedure can be considered.

- 1) Set margins  $p, v, a > 0$  based on robustness requirements.
- 2) Design reference trajectory  $\mathbf{q}_i^r, \dot{\mathbf{q}}_i^r, \ddot{\mathbf{q}}_i^r, i \in \mathcal{I}$  with the reference poses  $\mathbf{q}_i^r$  safely inside the static workspace [10].
- 3) Design hyperrectangular sets  $\mathcal{V}_c$  and  $\mathcal{A}_c$ , guaranteeing

$$\left\| \dot{\mathbf{q}}_i \right\|_\infty \leq v, \left\| \ddot{\mathbf{q}}_i \right\|_\infty \leq a \Rightarrow (\dot{\mathbf{q}}_i, \ddot{\mathbf{q}}_i) \in \mathcal{V}_c \times \mathcal{A}_c.$$

- 4) Derive the pose sets  $\mathcal{P}_i$  and check if the following holds:

$$\left\| \tilde{\mathbf{q}}_i \right\|_\infty \leq p \Rightarrow \mathbf{q}_i \in \mathcal{P}_i.$$

If it does, then Condition 4 is satisfied, otherwise slow down the reference trajectory (to relax the velocity/acceleration requirements) and go back to step 3).

It should be noted that the pose sets  $\mathcal{P}_i$  in the feasible pose corridor are independent of each other and also of  $\mathbf{x}_k$ . As such,

these sets can be precomputed offline for a given reference trajectory. Fig. 3(b) illustrates the schematic for such *offline workspace-based constraint convexification*. As will be shown in the following, the offline generated convex constraints allow the FLIMPC (13) to be efficiently convexified and solved. Details on the derivation of the workspace  $\mathcal{P}$  and the convex subsets  $\mathcal{P}_i$  for each time step are given in Section IV.

### C. Workspace-Based MPC Formulation

Theorem 1 and (18) provide a way to convexify the FLIMPC problem from (13). By combining (15) and (18), the convexified constraints can be expressed as

$$\begin{aligned} M_k \mathbf{v}_{k|k} + \mathbf{c}_k + \mathbf{g}_k &= -L_k^T \mathbf{f}_k, \mathbf{f}_k \in \mathcal{F} \\ \mathbf{X}_k &= A\mathbf{x}_k + B\mathbf{V}_k \\ \mathbf{X}_k &\in \mathcal{P}_{k+1} \times \mathcal{V}_c \times \cdots \times \mathcal{P}_{k+N} \times \mathcal{V}_c \\ \mathbf{V}_k &\in \mathbb{R}^n \times \mathcal{A}_c^{N-1}. \end{aligned} \quad (23)$$

On the other hand, the objective function of the MPC can be constructed by three parts: 1) tracking of reference state over the horizon; 2) tracking of reference virtual input over the horizon; and 3) cable force effort at the first step of the horizon, resulting in a convex and quadratic objective

$$\underset{\mathbf{X}_k, \mathbf{V}_k, \mathbf{f}_k}{\text{minimize}} \quad \|\mathbf{X}_k - \mathbf{X}_k^r\|_Q^2 + \|\mathbf{V}_k - \mathbf{V}_k^r\|_R^2 + \|\mathbf{f}_k\|_H^2 \quad (24)$$

where  $Q \succeq 0 \in \mathbb{R}^{2nN \times 2nN}$  is positive semi-definite, and  $R \succ 0 \in \mathbb{R}^{nN \times nN}$  and  $H \succ 0 \in \mathbb{R}^{m \times m}$  are positive definite weights.

Additionally, to offer recursive feasibility and stability guarantee [44], the terminal constraint/cost can also be included in W-MPC formulation to replace the corresponding terms in (23) and (24), which can be represented by

$$\begin{aligned} \text{terminal cost:} \quad &\|\mathbf{x}_{k+N|k} - \mathbf{x}_{k+N}^r\|_P^2 \\ \text{terminal constraint:} \quad &\mathbf{x}_{k+N|k} \in \phi_{k+N} \end{aligned} \quad (25)$$

with  $P \succ 0 \in \mathbb{R}^{2n \times 2n}$  being the terminal cost weight and  $\phi_{k+N} \subset \mathcal{P}_{k+N} \times \mathcal{V}_c$  being the convex terminal constraint set. Section III-D describes the design of these *terminal conditions* (constraints and cost) while Appendix A establishes the recursive feasibility and stability using these conditions.

Finally, the W-MPC can be formulated using (23) and (24)

$$\begin{aligned} \underset{\mathbf{X}_k, \mathbf{V}_k, \mathbf{f}_k}{\text{minimize}} \quad &\|\mathbf{X}_k - \mathbf{X}_k^r\|_Q^2 + \|\mathbf{V}_k - \mathbf{V}_k^r\|_R^2 + \|\mathbf{f}_k\|_H^2 \\ \text{subject to} \quad &M_k \mathbf{v}_{k|k} + \mathbf{c}_k + \mathbf{g}_k = -L_k^T \mathbf{f}_k, \mathbf{f}_k \in \mathcal{F} \\ &\mathbf{X}_k = A\mathbf{x}_k + B\mathbf{V}_k \\ &\mathbf{X}_k \in \mathcal{P}_{k+1} \times \mathcal{V}_c \times \cdots \times \mathcal{P}_{k+N-1} \times \mathcal{V}_c \times \phi_{k+N} \\ &\mathbf{V}_k \in \mathbb{R}^n \times \mathcal{A}_c^{N-1} \end{aligned} \quad (26)$$

where

$$Q = \text{diag}(\underbrace{\tilde{Q}, \dots, \tilde{Q}}_{N-1}, P), \quad R = \text{diag}(\underbrace{\tilde{R}, \dots, \tilde{R}}_N)$$

with  $\tilde{Q} \succeq 0 \in \mathbb{R}^{2n \times 2n}$  and  $\tilde{R} \succ 0 \in \mathbb{R}^{n \times n}$  being the weights for state error and virtual input error at an individual time step. While the workspace-based convexification only requires sets  $\mathcal{P}_i$ ,  $\mathcal{V}_c$ , and  $\mathcal{A}_c$  to be convex, they are designed/derived as hyperrectangles in practice, resulting in linear inequality (bounded) constraints, allowing (26) to be formulated as a QP.

#### D. Terminal Constraint/Cost Design

The design of terminal constraint/cost (25) corresponds to a terminal controller, which is assumed to take over the control beyond the MPC horizon ( $i \geq k + N$ ). A common choice for the terminal controller is a discrete LQR [45], [46], which is designed in correspondence to a linear system and a quadratic stage cost. Consider the discrete linear system (9) and a stage cost for any time step  $i > 0$

$$l_i(\mathbf{x}_i, \mathbf{v}_i) = \|\mathbf{x}_i - \mathbf{x}_i^r\|_Q^2 + \|\mathbf{v}_i - \mathbf{v}_i^r\|_R^2.$$

According to LQR control, a positive definite matrix  $P$  and a feedback gain  $K$  can be computed by solving the discrete algebraic Riccati equation

$$P = A_d^\top P A_d - (A_d^\top P B_d) \left( \tilde{R} + B_d^\top P B_d \right)^{-1} (B_d^\top P A_d) + \tilde{Q} \quad (27)$$

$$K = \left( \tilde{R} + B_d^\top P B_d \right)^{-1} B_d^\top P A_d$$

with a corresponding feedback control law defined by

$$\mathbf{v}_i = \kappa_i(\mathbf{x}_i) = \mathbf{v}_i^r - K(\mathbf{x}_i - \mathbf{x}_i^r). \quad (28)$$

Also considering the well-established properties of LQR (Properties 1–3), the corresponding terminal constraint/cost can be derived, as summarized in Remark 2. Lemma 1 shows the properties of the terminal constraint that are relevant to W-MPC, which are used to prove the controller's recursive feasibility and stability in Appendix A. It is worth noting that the terminal constraint/cost design is closely related to the workspace-based convexification with sets  $\mathcal{P}_i$ ,  $\mathcal{V}_c$ , and  $\mathcal{A}_c$  used.

*Property 1 (LQR Optimality):* Applying the control law (28) to LTI system (9) results in the following relationship:

$$V_i(\mathbf{x}_i) = V_{i+1}(\mathbf{x}_{i+1}) + l_i(\mathbf{x}_i, \mathbf{v}_i)$$

with  $\mathbf{x}_{i+1} = A_d \mathbf{x}_i + B_d \kappa_i(\mathbf{x}_i)$ ,  $\mathbf{v}_i = \kappa_i(\mathbf{x}_i)$ , and  $V_i(\mathbf{x}_i)$  representing an infinite horizon cost at time step  $i$

$$V_i(\mathbf{x}_i) = \|\mathbf{x}_i - \mathbf{x}_i^r\|_P^2 = \sum_{j=i}^{\infty} l_j(\mathbf{x}_j, \mathbf{v}_j). \quad (29)$$

*Property 2 (LQR Stability and Invariant Set):* For LTI system (9), the LQR (28) is asymptotically stable in tracking the reference trajectory. Moreover, there exists an invariant set

$$\tilde{\mathcal{X}}_\phi(\rho) = \{\tilde{\mathbf{x}} \in \mathbb{R}^{2n} \mid \|\tilde{\mathbf{x}}\|_P^2 \leq \rho\} \quad (30)$$

for the tracking error  $\tilde{\mathbf{x}} = \mathbf{x} - \mathbf{x}^r$  with  $\rho > 0$  such that once  $\tilde{\mathbf{x}}$  enters  $\tilde{\mathcal{X}}_\phi(\rho)$ , it will remain inside.

*Property 3 (LQR Input Boundedness):* For a tracking error invariant set  $\tilde{\mathcal{X}}_\phi(\rho)$  with  $\rho > 0$ , a corresponding invariant set

$\tilde{\mathcal{A}}_\phi(\rho)$  for the virtual input error  $\tilde{\mathbf{v}} = \mathbf{v} - \mathbf{v}^r$  can be defined as

$$\tilde{\mathcal{A}}_\phi(\rho) = \left\{ \tilde{\mathbf{v}} \in \mathbb{R}^n \mid \tilde{\mathbf{v}} = -K\tilde{\mathbf{x}}, \tilde{\mathbf{x}} \in \tilde{\mathcal{X}}_\phi(\rho) \right\} \quad (31)$$

such that once  $\tilde{\mathbf{v}}$  enters  $\tilde{\mathcal{A}}_\phi(\rho)$ , all the future virtual input errors will remain inside.

*Remark 2:* Assume that the workspace-based convexification in Theorem 1 is used, the terminal conditions (25) for the proposed W-MPC can be derived as follows.

- 1) The weight matrix  $P$  in the terminal cost is a symmetric positive definite matrix derived by solving (27).
- 2) The terminal constraint set  $\phi_{k+N}$  is defined by

$$\phi_{k+N} = \mathbf{x}_{k+N}^r \oplus \tilde{\mathcal{X}}_\phi(\rho_r)$$

where  $\oplus$  represents the Minkowski sum and  $\rho_r > 0$  is the maximum scalar satisfying

$$\begin{aligned} \mathbf{x}_i^r \oplus \tilde{\mathcal{X}}_\phi(\rho_r) &\subset \mathcal{P}_i \times \mathcal{V}_c \\ \mathbf{v}_i^r \oplus \tilde{\mathcal{A}}_\phi(\rho_r) &\subset \mathcal{A}_c \end{aligned} \quad (32)$$

for all time steps  $i$  on the trajectory reference. In practice, a convex inner polytope of  $\phi_{k+N}$  can be used to derive a linear constraint  $A_\phi \mathbf{x}_{k+N|k} \leq b_\phi$  to replace  $\mathbf{x}_{k+N|k} \in \phi_{k+N}$ .

*Lemma 1 (Terminal Control Law Feasibility):* By the terminal control law (28) and the terminal constraint from Remark 2, for time step  $k$ , the future predictions beyond the horizon satisfy ( $i \geq k + N$ )

$$\mathbf{x}_{i|k} \in \phi_i \subset \mathcal{P}_i \times \mathcal{V}_c, \mathbf{v}_{i|k} = \kappa_i(\mathbf{x}_{i|k}) \in \mathcal{A}_c. \quad (33)$$

*Proof:* Given that  $\mathbf{x}_{k+N|k} \in \phi_{k+N}$ , the corresponding state error at time step  $k + N$  satisfies

$$\tilde{\mathbf{x}}_{k+N|k} = \mathbf{x}_{k+N|k} - \mathbf{x}_{k+N}^r \in \tilde{\mathcal{X}}_\phi(\rho_r).$$

Moreover, from Properties 2 and 3, for any steps  $i \geq k + N$

$$\begin{aligned} \mathbf{x}_{i|k} - \mathbf{x}_i^r &= \tilde{\mathbf{x}}_{i|k} \in \tilde{\mathcal{X}}_\phi(\rho_r) \\ \mathbf{v}_{i|k} - \mathbf{v}_i^r &= \tilde{\mathbf{v}}_{i|k} \in \tilde{\mathcal{A}}_\phi(\rho_r). \end{aligned}$$

Since (32) holds and the virtual input is assumed to be always determined by (28), then (33) is satisfied. ■

#### IV. W-MPC WORKSPACE AND FEASIBLE POSE CORRIDOR GENERATION

For the W-MPC workspace  $\mathcal{P}$  satisfying (20), it is possible to come up with conditions to check if a pose  $\mathbf{q}$  is inside  $\mathcal{P}$

$$\text{cond}_s(\mathbf{q}) \wedge \text{cond}_i(\mathbf{q}) \iff \mathbf{q} \in \mathcal{P}$$

with  $\text{cond}_s(\mathbf{q})$  and  $\text{cond}_i(\mathbf{q})$  being conditions related to the state and virtual input constraints, respectively, and

$$\text{cond}_s(\mathbf{q}) \iff \forall \dot{\mathbf{q}} \in \mathcal{V}_c : (\mathbf{q}, \dot{\mathbf{q}}) \in \mathcal{X}$$

$$\text{cond}_i(\mathbf{q}) \iff \forall \dot{\mathbf{q}} \in \mathcal{V}_c : \mathcal{A}_c \subset \mathcal{A}(\mathbf{q}, \dot{\mathbf{q}}) = \mathcal{A}(\mathbf{x}). \quad (34)$$

In practice, it can be computationally difficult to verify the above conditions due to the infinite number of possible  $\dot{\mathbf{q}}$ . Hence,

instead of using (34), easily verifiable forms of  $\text{cond}_s(\mathbf{q})$  and  $\text{cond}_i(\mathbf{q})$  can be designed to guarantee

$$\text{cond}_s(\mathbf{q}) \Rightarrow \forall \dot{\mathbf{q}} \in \mathcal{V}_c : (\mathbf{q}, \dot{\mathbf{q}}) \in \mathcal{X} \quad (35a)$$

$$\text{cond}_i(\mathbf{q}) \Rightarrow \forall \dot{\mathbf{q}} \in \mathcal{V}_c : \mathcal{A}_c \subset \mathcal{A}(\mathbf{q}, \dot{\mathbf{q}}). \quad (35b)$$

One consequence of using (35) is that the combined feasibility condition will be conservative, which only guarantees

$$\text{cond}_s(\mathbf{q}) \wedge \text{cond}_i(\mathbf{q}) \Rightarrow \mathbf{q} \in \mathcal{P}.$$

Although it is possible to derive an estimation of set  $\mathcal{P}$  using these conditions, the result is most likely nonconvex and will not be directly used to formulate W-MPC. Alternatively, hyperrectangular subsets (Definition 1) are derived using a *point-wise method*, which can be further combined into the feasible pose corridor (Definition 2) for a given trajectory.

#### A. State Workspace Constraint ( $\text{cond}_s$ )

The feasible state set  $\mathcal{X}$  from (35a) is a state-space region confining both joint pose and velocity, and arises from various state constraints as required by the specific problem. Two common examples include the workspace considering no cable interference and the satisfaction of cable velocity bounds.

1) *Cable Interference Avoidance*: For CDRs, avoiding cable–cable collisions is important. As shown in [40], the cable interference-free condition can be formulated into a closed-form function of the joint pose and can be used to verify  $\text{cond}_s(\mathbf{q})$ , where

$$\text{cond}_s(\mathbf{q}) = \begin{cases} 1, & \text{no cable interference} \\ 0, & \text{cable interference} \end{cases}$$

2) *Cable Velocity Bound*: Since the actuating cables in CDRs are typically driven by motors, cable velocity bounds exist, which can be denoted by  $\dot{\mathbf{i}}_{\min}$  and  $\dot{\mathbf{i}}_{\max}$  for the minimum and maximum cable velocity vectors, respectively. Using the *twist feasible* condition proposed in [47], the satisfaction of the desired joint velocity set  $\dot{\mathbf{q}} \in \mathcal{V}_c$  can be computed by evaluating

$$\text{cond}_s(\mathbf{q}) = \begin{cases} 1, & \mathcal{V}_c \subset \mathcal{T}(\mathbf{q}) \\ 0, & \text{otherwise} \end{cases}$$

where  $\mathcal{T}(\mathbf{q}) = \{\dot{\mathbf{q}} \in \mathbb{R}^n \mid \dot{\mathbf{i}}_{\min} \leq L(\mathbf{q})\dot{\mathbf{q}} \leq \dot{\mathbf{i}}_{\max}\}$ .

#### B. Dynamic Feasible Workspace Constraint ( $\text{cond}_i$ )

Assume that sets  $\mathcal{V}_c$  and  $\mathcal{A}_c$  are convex polytopes that are determined by the system capability and task requirement, refer to explanations in Section III-B and examples in Section V-A1,  $\text{cond}_i(\mathbf{q})$  should satisfy

$$\forall \dot{\mathbf{q}} \in \mathcal{V}_c : \mathcal{A}_c \subset \mathcal{A}(\mathbf{q}, \dot{\mathbf{q}}). \quad (36)$$

As directly evaluating (36) is computationally intractable with infinitely many joint velocities existing in  $\mathcal{V}_c$ , an easily verifiable sufficient condition for (36) will be used instead.

Considering the definition of  $\mathcal{A}(\mathbf{q}, \dot{\mathbf{q}})$  in (11), (36) can be equivalently formulated into the form

$$\forall (\dot{\mathbf{q}}, \ddot{\mathbf{q}}) \in \mathcal{V}_c \times \mathcal{A}_c, \exists \mathbf{f} \in \mathcal{F} : \mathbf{w}_r(\mathbf{q}, \dot{\mathbf{q}}, \ddot{\mathbf{q}}) = -L^\top(\mathbf{q})\mathbf{f} \quad (37)$$

where  $\mathbf{w}_r(\mathbf{q}, \dot{\mathbf{q}}, \ddot{\mathbf{q}})$  is the required wrench to produce  $\ddot{\mathbf{q}}$  at  $(\mathbf{q}, \dot{\mathbf{q}})$

$$\mathbf{w}_r(\mathbf{q}, \dot{\mathbf{q}}, \ddot{\mathbf{q}}) = M(\mathbf{q})\ddot{\mathbf{q}} + \mathbf{c}(\mathbf{q}, \dot{\mathbf{q}}) + \mathbf{g}(\mathbf{q}).$$

For a given  $\mathbf{q}$ , a required wrench set  $\mathcal{W}_r(\mathbf{q})$  can be defined by

$$\mathcal{W}_r(\mathbf{q}) = \{\mathbf{w} \in \mathbb{R}^n \mid \mathbf{w} = \mathbf{w}_r(\mathbf{q}, \dot{\mathbf{q}}, \ddot{\mathbf{q}}), \exists (\dot{\mathbf{q}}, \ddot{\mathbf{q}}) \in \mathcal{V}_c \times \mathcal{A}_c\}$$

covering the necessary wrenches for (36) to hold at pose  $\mathbf{q}$ . On the other hand, the actuation constraint  $\mathbf{f} \in \mathcal{F}$  results in an available wrench set

$$\mathcal{W}_a(\mathbf{q}) = \{\mathbf{w} \in \mathbb{R}^n \mid \mathbf{w} = -L^\top(\mathbf{q})\mathbf{f}, \exists \mathbf{f} \in \mathcal{F}\}.$$

Consequently, (37) can be equivalently expressed as

$$\mathcal{W}_r(\mathbf{q}) \subset \mathcal{W}_a(\mathbf{q}). \quad (38)$$

In general, verifying continuous set inclusion  $\mathcal{S}_1 \subset \mathcal{S}_2$  is still an intractable problem unless both  $\mathcal{S}_1$  and  $\mathcal{S}_2$  are convex. In fact, for computational efficiency and algorithm generality, it is desirable for  $\mathcal{S}_1$  to be a convex polytope, in which case

$$\mathcal{S}_1 \subset \mathcal{S}_2 \iff \text{vertex}(\mathcal{S}_1) \subset \mathcal{S}_2$$

with  $\text{vertex}(\cdot)$  representing the vertices of the given convex polytope. In this particular case, while  $\mathcal{W}_a(\mathbf{q})$  is a convex zonotope [48], [49],  $\mathcal{W}_r(\mathbf{q})$  is typically nonconvex for non-zero centrifugal/Coriolis terms  $\mathbf{c}(\mathbf{q}, \dot{\mathbf{q}})$  and hence condition (38) cannot be easily verified. However, by deriving a convex polytope  $\mathcal{W}_{ro}(\mathbf{q})$  that is a superset of  $\mathcal{W}_r(\mathbf{q})$ , an easily verifiable sufficient condition for (38) can be defined

$$\mathcal{W}_{ro}(\mathbf{q}) \subset \mathcal{W}_a(\mathbf{q}) \iff \text{vertex}(\mathcal{W}_{ro}(\mathbf{q})) \subset \mathcal{W}_a(\mathbf{q}). \quad (39)$$

In order to derive  $\mathcal{W}_{ro}(\mathbf{q})$ , the following decomposition of  $\mathcal{W}_r(\mathbf{q})$  will be considered:

$$\mathcal{W}_r(\mathbf{q}) = \mathcal{W}_A(\mathbf{q}) \oplus \mathcal{W}_V(\mathbf{q}) \oplus \mathbf{g}(\mathbf{q})$$

where

$$\mathcal{W}_A(\mathbf{q}) = \{\mathbf{w} \in \mathbb{R}^n \mid \mathbf{w} = M(\mathbf{q})\ddot{\mathbf{q}}, \exists \ddot{\mathbf{q}} \in \mathcal{A}_c\}$$

$$\mathcal{W}_V(\mathbf{q}) = \{\mathbf{w} \in \mathbb{R}^n \mid \mathbf{w} = \mathbf{c}(\mathbf{q}, \dot{\mathbf{q}}), \exists \dot{\mathbf{q}} \in \mathcal{V}_c\}.$$

Since  $\mathcal{V}_c$  and  $\mathcal{A}_c$  are convex polytopes, the only potentially nonconvex set is  $\mathcal{W}_V(\mathbf{q})$ , an image of a nonlinear mapping of the set  $\mathcal{V}_c$ . Hence, the key to finding  $\mathcal{W}_{ro}(\mathbf{q})$  is to obtain a convex superset of  $\mathcal{W}_V(\mathbf{q})$ . To achieve the goal, the special structure of the centrifugal/Coriolis term  $\mathbf{c}(\mathbf{q}, \dot{\mathbf{q}})$  is exploited, which can be written into a quadratic form [50]

$$\mathbf{c}(\mathbf{q}, \dot{\mathbf{q}}) = \begin{bmatrix} \dot{\mathbf{q}}^\top \mathbf{N}_1(\mathbf{q}) \dot{\mathbf{q}} \\ \vdots \\ \dot{\mathbf{q}}^\top \mathbf{N}_n(\mathbf{q}) \dot{\mathbf{q}} \end{bmatrix}. \quad (40)$$

Terms  $\mathbf{N}_i(\mathbf{q})$ ,  $i = 1, \dots, n$  are square matrices computed by applying second order algorithmic differentiation [51] to the recursive Newton–Euler algorithm [52], which forms a subroutine denoted as `modifiedRNEA()`. On the other hand, a minimum volume enclosing ellipsoid of  $\mathcal{V}_c$  can be defined as

$$\mathcal{E}_V = \{\mathbf{y} \in \mathbb{R}^n \mid \mathbf{y} = E_V \mathbf{r}, \exists \mathbf{r} \in \mathbb{R}^n \text{ s.t. } \|\mathbf{r}\| \leq 1\} \quad (41)$$

**Algorithm 1:** Centrifugal/Coriolis Force Bound Derivation.

---

**Input:**  $\mathbf{q}, E_v$   
**Output:**  $\mathcal{W}_{Ve}(\mathbf{q})$   
 $n \leftarrow \text{length}(\mathbf{q})$   
 $N_1, N_2, \dots, N_n \leftarrow \text{modifiedRNEA}(\mathbf{q})$   
**for**  $i = 1$  to  $n$  **do**  
     $\lambda_{\max}, \lambda_{\min} \leftarrow \text{eigenvalue}(E_v^T(N_i + N_i^T)E_v/2)$   
     $c_{\min}(i) \leftarrow \min(0, \lambda_{\min})$   
     $c_{\max}(i) \leftarrow \max(0, \lambda_{\max})$   
**end for**  
**return**  $[c_{\min}, c_{\max}]$

---

satisfying  $\mathcal{V}_c \subset \mathcal{E}_V$ . In particular, the matrix  $E_v$  that defines the ellipsoid (41) can be computed using [53]. Based on the velocity ellipsoid (41), a bounding set of (40) is derived as  $\mathcal{W}_{Ve}$  using Algorithm 1, satisfying  $\mathcal{W}_V(\mathbf{q}) \subset \mathcal{W}_{Ve}(\mathbf{q})$ .

From  $\mathcal{W}_{Ve}(\mathbf{q})$ , a superset  $\mathcal{W}_{ro}(\mathbf{q})$  can be derived as the following convex polytope:

$$\mathcal{W}_{ro}(\mathbf{q}) = \mathcal{W}_A(\mathbf{q}) \oplus \mathcal{W}_{Ve}(\mathbf{q}) \oplus g(\mathbf{q}). \quad (42)$$

This allows (39) to be used as  $\text{cond}_i(\mathbf{q})$

$$\text{cond}_i(\mathbf{q}) \iff \text{vertex}(\mathcal{W}_{ro}(\mathbf{q})) \subset \mathcal{W}_a(\mathbf{q}) \quad (43)$$

which guarantees (35b) to hold. For  $\mathcal{W}_{ro}(\mathbf{q})$  with  $p$  vertices, only  $p$  linear programs need to be solved to verify (43).

**C. Maximum Workspace Hyperrectangle Derivation**

From Theorem 1, W-MPC involves the derivation of the feasible pose corridor (Definition 2), composed of a series of maximum workspace hyperrectangles (Definition 1) centered at each reference pose. A generic *hyperrectangular neighborhood* of point  $\mathbf{q}$  can be defined as

$$\mathcal{C}(\mathbf{q}, r, \delta\mathbf{q}) = \left\{ \mathbf{y} \in \mathbb{R}^n \mid \mathbf{q} - \frac{r}{2}\delta\mathbf{q} \leq \mathbf{y} \leq \mathbf{q} + \frac{r}{2}\delta\mathbf{q} \right\} \quad (44)$$

where  $\delta\mathbf{q}$  determines the shape of  $\mathcal{C}(\mathbf{q}, r, \delta\mathbf{q})$  with  $\min(\delta\mathbf{q}) > 0$ ,  $\max(\delta\mathbf{q}) = 1$ , and  $r > 0$  is scaling parameter that adjusts the size of  $\mathcal{C}(\mathbf{q}, r, \delta\mathbf{q})$ . In practice, each element of  $\delta\mathbf{q}$  shall be defined by the user based on the desired system behavior, e.g., smaller values shall be taken on DoFs that are expected to have relatively tight tracking. The derivation of the maximum workspace hyperrectangle then becomes finding the maximum scaling parameter  $r$  for a hyperrectangular neighborhood  $\mathcal{C}(\mathbf{q}, r, \delta\mathbf{q})$  centered at a given pose  $\mathbf{q}$  such that the hyperrectangular neighborhood is completely inside the W-MPC workspace. Algorithm 2 presents such a way to determine the maximum workspace hyperrectangle through bisection. The inputs of Algorithm 2 include a center point  $\mathbf{q}$ , a small positive value  $\epsilon$  as the hyperrectangle size tolerance, and a large scalar  $R > 0$  as the largest possible hyperrectangle size.

Note that Algorithm 2 requires a `setFeasible()` subroutine to check the feasibility of a continuous set. A *point-wise approach* is commonly used in the CDR workspace studies to tackle such problem, where the continuous set's feasibility

**Algorithm 2:** Maximum Workspace Hyperrectangle Derivation:

---

**Input:**  $\mathbf{q}, \epsilon, R, \delta\mathbf{q}$   
**Output:**  $\mathcal{C}$   
 $r_{\min} \leftarrow 0, r_{\max} \leftarrow R$   
**if not** `setFeasible`( $\mathcal{C}(\mathbf{q}, r_{\min}, \delta\mathbf{q})$ ) **then**  
    **return**  $\emptyset$   
**else if** `setFeasible`( $\mathcal{C}(\mathbf{q}, r_{\max}, \delta\mathbf{q})$ ) **then**  
    **return**  $\mathcal{C}(\mathbf{q}, r_{\max}, \delta\mathbf{q})$   
**else**  
    **while**  $|r_{\min} - r_{\max}| > \epsilon$  **do**  
         $r \leftarrow (r_{\min} + r_{\max})/2$   
        **if** `setFeasible`( $\mathcal{C}(\mathbf{q}, r, \delta\mathbf{q})$ ) **then**  
             $r_{\min} \leftarrow r$   
        **else**  
             $r_{\max} \leftarrow r$   
        **end if**  
    **end while**  
    **return**  $\mathcal{C}(\mathbf{q}, r_{\min}, \delta\mathbf{q})$   
**end if**

---

**Algorithm 3:** Point-Wise Set Feasibility Evaluation:

---

// An implementation of subroutine `setFeasible()`  
**Input:**  $\mathcal{S}$   
**Output:** {true, false}  
 $\mathcal{S}_p \leftarrow \text{sampling}(\mathcal{S})$   
**while**  $\mathcal{S}_p \neq \emptyset$  **do**  
    randomly select  $\mathbf{q} \in \mathcal{S}_p$   
    **if**  $\text{cond}_s(\mathbf{q}) \wedge \text{cond}_i(\mathbf{q})$  **then**  
         $\mathcal{S}_p = \mathcal{S}_p \setminus \{\mathbf{q}\}$   
    **else**  
        **return** false  
    **end if**  
**end while**  
**return** true

---

is estimated using the feasibility of a sample set with a finite number of elements. Using a *uniform grid*, the subroutine `sampling()` returns a set of grid points that are covered by the input set. Combining the sampling subroutine `sampling()` and the conservative feasibility condition  $\text{cond}_s(\mathbf{q}) \wedge \text{cond}_i(\mathbf{q})$ , a *conservative* feasibility estimation of a given continuous set can be derived using Algorithm 3.

Combining Algorithms 1–3, a hyperrectangle centered at  $\mathbf{q}$  inside the workspace  $\mathcal{P}$  is generated. Repeating for every pose  $\mathbf{q}_i^r$  on the reference trajectory, the feasible pose corridor for the W-MPC can be determined. Note that parameter  $R$  in Algorithm 2 also affects the conservativeness of the resulting hyperrectangles, where a smaller  $R$  reduces the computational load, together with the size of the resulting sets.

**V. SIMULATION RESULTS**

The performance of the proposed W-MPC is illustrated by the simulation of two different CDRs in this section, including

TABLE I  
DYNAMIC FEASIBLE WORKSPACE PARAMETERS FOR 2-R PLANAR CABLE ROBOT

	Allowed Velocity ( $\mathcal{V}_c$ )	Allowed Acceleration ( $\mathcal{A}_c$ )	Available Force ( $\mathcal{F}$ )
DFW <sub>1</sub>	$\dot{q}_1, \dot{q}_2 \in [-1.0, 1.0]$ rad/sec	$\ddot{q}_1, \ddot{q}_2 \in [-2.0, 2.0]$ rad/sec <sup>2</sup>	$f_1, f_2, f_3, f_4 \in [10, 100]$ N
DFW <sub>2</sub>	$\dot{q}_1, \dot{q}_2 \in [-8.0, 8.0]$ rad/sec	$\ddot{q}_1, \ddot{q}_2 \in [-16, 16]$ rad/sec <sup>2</sup>	$f_1, f_2, f_3, f_4 \in [10, 100]$ N

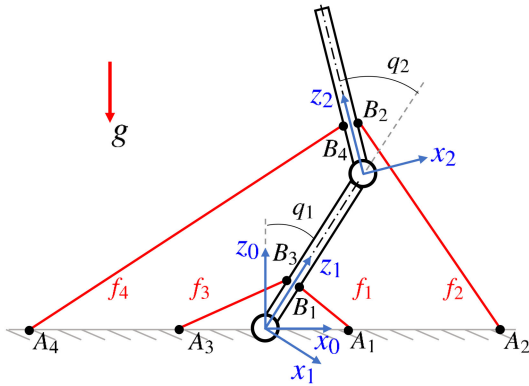


Fig. 5. 2-Link cable-driven robot.

a 2-DoF multilink robot and a 6-DoF spatial cable robot, for both nominal and non-nominal cases. Simulations were performed using the CASPR software [39] on a computer with an Intel Core i7-7700 K processor with 16 GBs of memory and MATLAB version 2020a. The controller ran at 200 Hz, and the QPs were solved with qpOASES [54]. Comparison with constant gain CTC was also made to show the advantages of the proposed W-MPC. Although other more complex nonlinear control laws exist, such as the Slotine-Li controller [55], they are not fundamentally different from CTC in terms of input constraint handling. In fact, a shared drawback of these nonlinear control laws is the lack of constraint handling capability, which can be well illustrated by CTC.

#### A. 2-DoF Multilink CDR

A simple 2-DoF CDR (Fig. 5) is used to illustrate different aspects of the W-MPC, including 1) the design of the dynamic feasible workspace (DFW) and the reference trajectories; 2) the control performance under several non-nominal scenarios; and 3) the performance impact of some key controller settings. The example CDR has four actuating cables and two identical links, each being 1 m in length with the following properties:

$$m_1 = m_2 = 0.1 \text{ kg}, G_1 = G_2 = (0, 0, 0.5) \text{ m}$$

$$I_1 = I_2 = \text{diag}(0.083, 0, 0.083) \text{ kg m}^2$$

where  $G_1, G_2$  are the locations of each link's center of mass defined in its local frame. The cable attachment locations are

$$A_1 = -A_3 = (0.5, 0.005, 0) \quad A_2 = -A_4 = (1.5, 0.005, 0)$$

$$B_1 = B_2 = (0.1, 0.05, 0.3) \quad B_3 = B_4 = (-0.1, -0.05, 0.3)$$

where  $B_1, \dots, B_4$  are defined in the corresponding link's local frame, and  $A_1, \dots, A_4$  are defined in the base frame.

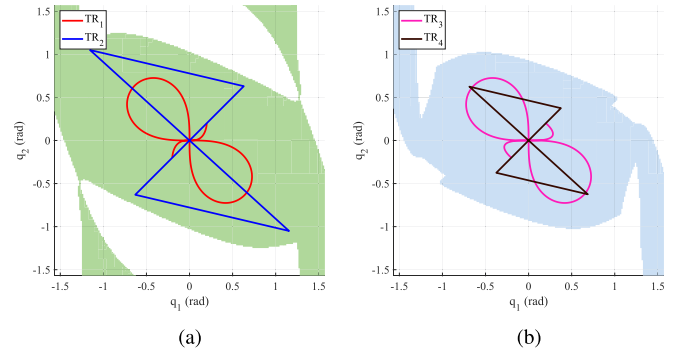


Fig. 6. Different dynamic feasible workspaces and reference trajectories. (a) DFW<sub>1</sub> with TR<sub>1</sub> and TR<sub>2</sub>. (b) DFW<sub>2</sub> with TR<sub>3</sub> and TR<sub>4</sub>.

#### 1) W-MPC Workspace and Reference Trajectory Design:

As introduced in Section III-B, the design of the reference trajectories is intertwined with the W-MPC workspace design, where Condition 4 must be satisfied. Only the DFW constraint (Section IV-B) was considered in this example, with two different DFW settings DFW<sub>1</sub> and DFW<sub>2</sub> (shown in Table I). In Fig. 6, the workspaces DFW<sub>1</sub> and DFW<sub>2</sub> are visualized as the shaded regions. The primary difference between the two workspaces is that DFW<sub>2</sub> has a larger range of allowable velocities and accelerations, and hence can support faster and more dynamic trajectories. However, due to the same cable force availability (Table I), only joint poses with larger wrench capability can support the velocity and acceleration requirements of DFW<sub>2</sub>. Consequently, DFW<sub>2</sub> covers a smaller area in the joint space than DFW<sub>1</sub> [as illustrated in Fig. 6(b)] and only supports a more limited selection of paths for the CDR. While only DFW is considered in Fig. 6 for simplicity, the process of adding state constraint workspaces can be quite straightforward, where a filter shall be added to remove the poses in DFW that violate the state constraints.

In DFW<sub>1</sub> and DFW<sub>2</sub>, four trajectories were defined, as shown in Fig. 6. Trajectories TR<sub>1</sub> and TR<sub>3</sub> are smooth trajectories, while TR<sub>2</sub> and TR<sub>4</sub> are composed of several point-to-point constant-velocity segments. Trajectories TR<sub>1</sub> and TR<sub>3</sub> have almost identical paths, where TR<sub>1</sub> finishes the whole motion in 10 s while TR<sub>3</sub> has higher speed and completes the motion in 5.5 s. As shown in Fig. 7(c) and (d), TR<sub>3</sub> can only be supported by DFW<sub>2</sub> due to the higher velocity/acceleration demands. On the other hand, when trajectories have similar velocity/acceleration requirements, e.g., TR<sub>2</sub> and TR<sub>4</sub>, a larger motion range is allowed for reference trajectories in DFW<sub>1</sub>, as long as the corresponding velocity/acceleration limitations are satisfied. The selection of sets  $\mathcal{V}_c$  and  $\mathcal{A}_c$  directly affects both the motion range and the speed of the reference trajectory, hence a compromise

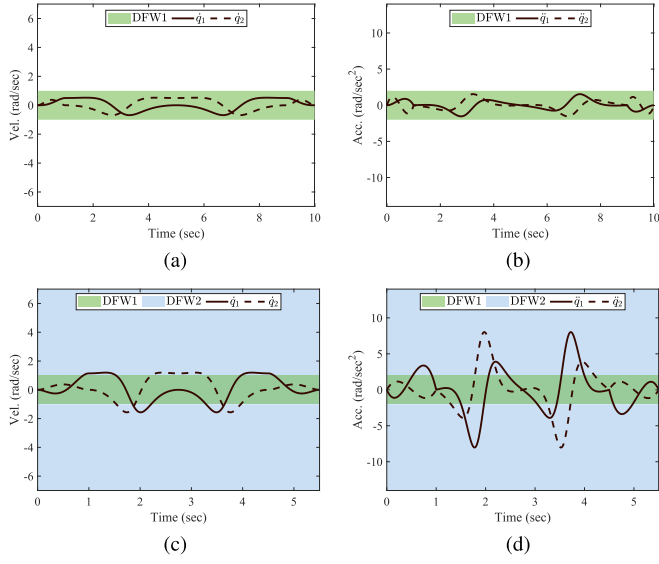


Fig. 7. Joint velocities and accelerations of trajectories TR<sub>1</sub> and TR<sub>3</sub>. (a) Joint velocities of TR<sub>1</sub>. (b) Joint accelerations of TR<sub>1</sub>. (c) Joint velocities of TR<sub>3</sub>. (d) Joint accelerations of TR<sub>3</sub>.

needs to be made where trajectories requiring higher velocity and acceleration capabilities shall be confined within a smaller set of poses. Moreover, based on Theorem 1, a larger margin between the boundaries of  $(\mathcal{P}_i, \mathcal{V}_c, \mathcal{A}_c)$  and reference trajectory  $(\mathbf{q}_i^r, \dot{\mathbf{q}}_i^r, \ddot{\mathbf{q}}_i^r)$  is desirable for a better robustness; in fact, if the reference trajectory gets too close to the workspace boundary, infeasibility can easily happen. For computational simplicity, sets  $(\mathcal{P}_i)$  are derived as hyperrectangles, forming bounds on each DoF, as illustrated by the unshaded area in Fig. 8 for TR3 and TR4. In particular, the unshaded area in Fig. 8(a) and (d) is effectively the feasible pose corridor.

2) *W-MPC Controller Performance*: In this example, the proposed controller was applied on TR<sub>3</sub> and TR<sub>4</sub> within DFW<sub>2</sub>. For the W-MPC constraints (23), the allowed velocity set  $\mathcal{V}_c$ , acceleration set  $\mathcal{A}_c$ , and force bounds  $\mathcal{F}$  are shown in Table I. The allowed pose sets  $\mathcal{P}_i$  for each time step  $i$  were determined as the maximum workspace hyperrectangles (Definition 1) centered at the reference pose  $\mathbf{q}_i^r$  using Algorithm 2. For objective (24), the weight matrices for the state error ( $\tilde{Q}$ ), the virtual input error ( $\tilde{R}$ ), and cable forces ( $H$ ) were

$$\tilde{Q} = \text{diag}(1, 1, 0, 0), \quad \tilde{R} = 10^{-10} \times I_{2 \times 2}, \quad H = 10^{-10} \times I_{4 \times 4}. \quad (45)$$

With a horizon of  $N = 50$ , the results of the W-MPC performing reference tracking of TR<sub>3</sub> and TR<sub>4</sub> subject to an initial pose error [0.3, 0.3] rad are shown in Fig. 8. The results show that the W-MPC was able to stably track both reference trajectories while satisfying all of the constraints.

It should be noted that the terminal constraint and cost were applied in the tracking of TR<sub>3</sub> and TR<sub>4</sub> (Fig. 8) to enforce the recursive feasibility and stability. However, in some non-nominal scenarios, the terminal constraint may seem to be overly strict and often cause control failure due to infeasibility. In such cases, W-MPC without terminal constraint/cost can also be applied. For example, in Fig. 9, a constant wrench disturbance

$\mathbf{w}_e = [1, -1]^T \text{N m}$  was applied during the TR<sub>3</sub> tracking with  $N = 10$  and no terminal constraint/cost. Despite having a relatively larger tracking error than the nominal case, the tracking control was still feasible and stable.

Next, the impact of the horizon length  $N$  and the use of terminal constraint/cost on W-MPC performance are investigated. Table II summarizes the performance of the controller with various settings for four different trajectory scenarios: 1) TR<sub>3</sub> without initial pose error; 2) TR<sub>3</sub> with an initial pose error of [0.3, 0.3] rad; 3) TR<sub>4</sub> with an initial pose error of [0.3, 0.3] rad; and 4) TR<sub>3</sub> subject to a constant disturbance wrench  $\mathbf{w}_e = [1, -1]^T \text{N m}$ . The W-MPC performance was quantified by the average joint tracking error norm (tracking error) and the average cable force vector norm (control effort).

From the results, when subject to an initial pose error and velocity error, with the latter being caused by the discontinuity of the reference velocity profile in TR<sub>4</sub>, the horizon length  $N$  must be sufficiently large such that the W-MPC is feasible with the terminal constraints. Similar observation can be made in the presence of large disturbances. On the other hand, without the terminal constraint/cost, the W-MPC performed similarly compared to the case with terminal constraint/cost under long horizon. Under short horizon, the absence of terminal constraint/cost allowed W-MPC to remain practically feasible, and presented a tighter tracking and better robustness. Computation-wise, Table III shows a significant increase of time cost for a larger  $N$ . As such, it is considered favorable in practice to employ W-MPC without the terminal constraint/cost under a relatively short horizon. For the remaining simulations, a horizon length of  $N = 10$  without the terminal constraint/cost was used.

3) *Comparison With Constant Gain CTC*: In CDR control, the most common approach is to use a CTC scheme with constant gains. For the constant gain CTC, the desired joint acceleration can be expressed as

$$\ddot{\mathbf{q}}_{\text{CTC}} = \ddot{\mathbf{q}}^r + K_d (\dot{\mathbf{q}}^r - \dot{\mathbf{q}}) + K_p (\mathbf{q}^r - \mathbf{q})$$

where  $\mathbf{q}^r$ ,  $\dot{\mathbf{q}}^r$ , and  $\ddot{\mathbf{q}}^r$  are the reference pose, joint velocity, and acceleration vectors, respectively. The matrices  $K_p \succeq 0$  and  $K_d \succeq 0$  are the proportional and differential gains, respectively. The corresponding cable forces satisfying the constraints can then be computed with inverse dynamics algorithms if the desired acceleration  $\ddot{\mathbf{q}}_{\text{CTC}}$  is feasible.

Despite the simplicity, CTC easily suffers from infeasibility when the tracking errors  $(\dot{\mathbf{q}}^r - \dot{\mathbf{q}})$  and  $(\mathbf{q}^r - \mathbf{q})$  become too large. This is mainly due to the lack of consideration of cable force bounds in determining the desired joint acceleration  $\ddot{\mathbf{q}}_{\text{CTC}}$  such that the inverse dynamics problem is infeasible. In contrast, the proposed W-MPC strictly follows the cable force constraints when selecting the joint acceleration to avoid infeasibility. To compare the performances of constant gain CTC and W-MPC, the tracking of TR<sub>3</sub> and TR<sub>4</sub> under both the *nominal scenario* and *external disturbance* were simulated.

In the comparison, DFW<sub>2</sub> was used to generate the joint pose, velocity, and acceleration constraints for the W-MPC. Two sets of gains were selected for the constant gain CTC with the low gain tuned to produce less aggressive control action to avoid infeasibility and high gain tuned to provide tighter tracking with

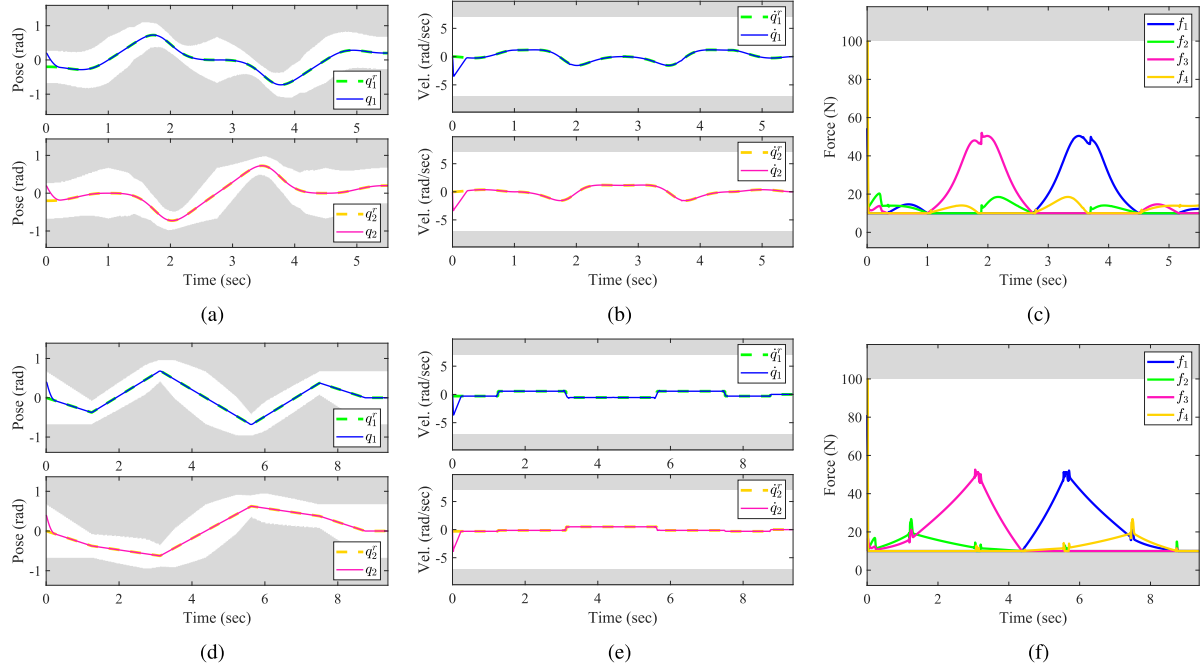


Fig. 8. TR<sub>3</sub> and TR<sub>4</sub> tracking with initial pose error  $\mathbf{e}_0 = [0.3, 0.3]$  rad ( $N = 90$ , with terminal constraint/cost). (a) Joint pose tracking of TR<sub>3</sub>. (b) Joint velocity tracking of TR<sub>3</sub>. (c) Cable forces of TR<sub>3</sub>. (d) Joint pose tracking of TR<sub>4</sub>. (e) Joint velocity tracking of TR<sub>4</sub>. (f) Cable forces of TR<sub>4</sub>.

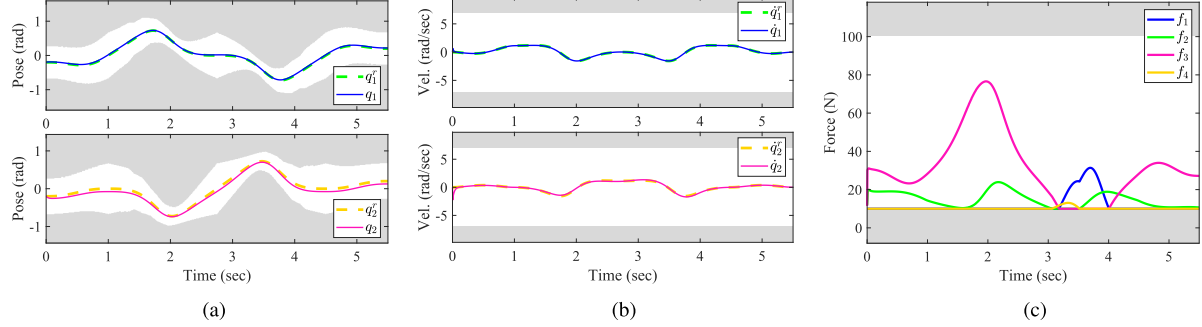


Fig. 9. TR<sub>3</sub> tracking under disturbance ( $\mathbf{w}_e = [1, -1]^T \text{N m}$ ) ( $N = 10$ , without terminal constraint/cost). (a) Joint pose tracking of TR<sub>3</sub>. (b) Joint velocity tracking of TR<sub>3</sub>. (c) Cable forces of TR<sub>3</sub>.

TABLE II  
PERFORMANCE COMPARISON OF W-MPC WITH PARAMETER VARIATION

		with terminal constraint and cost			without terminal constraint and cost		
		<b>N = 10</b>	<b>N = 50</b>	<b>N = 90</b>	<b>N = 10</b>	<b>N = 50</b>	<b>N = 90</b>
Trajectory TR <sub>3</sub> (without initial error)	error	$2.79 \cdot 10^{-4}$	$8.10 \cdot 10^{-4}$	$1.13 \cdot 10^{-3}$	$2.79 \cdot 10^{-4}$	$8.10 \cdot 10^{-4}$	$1.13 \cdot 10^{-2}$
	effort	$3.19 \cdot 10^1$	$3.19 \cdot 10^1$	$3.19 \cdot 10^1$	$3.19 \cdot 10^1$	$3.19 \cdot 10^1$	$3.19 \cdot 10^1$
Trajectory TR <sub>3</sub> (with initial error)	error	<b>infeasible</b>	<b>infeasible</b>	$9.83 \cdot 10^{-3}$	$5.43 \cdot 10^{-3}$	$9.45 \cdot 10^{-3}$	$9.83 \cdot 10^{-3}$
	effort	<b>infeasible</b>	<b>infeasible</b>	$3.23 \cdot 10^1$	$3.28 \cdot 10^1$	$3.23 \cdot 10^1$	$3.23 \cdot 10^1$
Trajectory TR <sub>4</sub> (with initial error)	error	<b>infeasible</b>	<b>infeasible</b>	$6.85 \cdot 10^{-3}$	$3.95 \cdot 10^{-3}$	$6.44 \cdot 10^{-3}$	$6.85 \cdot 10^{-2}$
	effort	<b>infeasible</b>	<b>infeasible</b>	$3.28 \cdot 10^1$	$3.30 \cdot 10^1$	$3.28 \cdot 10^1$	$3.28 \cdot 10^1$
Trajectory TR <sub>3</sub> (disturbance $\mathbf{w}_e = [1, -1]^T \text{N m}$ )	error	<b>infeasible</b>	$1.39 \cdot 10^{-1}$	$1.36 \cdot 10^{-1}$	$6.14 \cdot 10^{-2}$	$1.36 \cdot 10^{-1}$	$1.36 \cdot 10^{-1}$
	effort	<b>infeasible</b>	$4.24 \cdot 10^1$	$4.24 \cdot 10^1$	$4.02 \cdot 10^1$	$4.24 \cdot 10^1$	$4.24 \cdot 10^1$

TABLE III  
TIME COST COMPARISON

	median (ms)	range (ms)
CTC	0.4051	[0.3694, 0.9081]
W-MPC: N=10	0.6191	[0.5597, 1.3855]
W-MPC: N=50	3.9253	[3.0211, 6.3004]
W-MPC: N=90	15.2263	[13.7492, 36.0068]

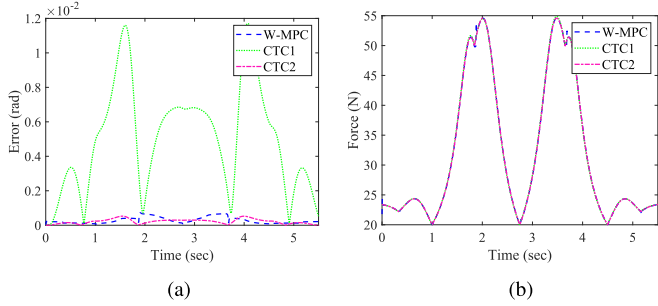


Fig. 10. Performance comparison: TR<sub>3</sub> nominal. (a) Tracking error norm. (b) Force vector norm.

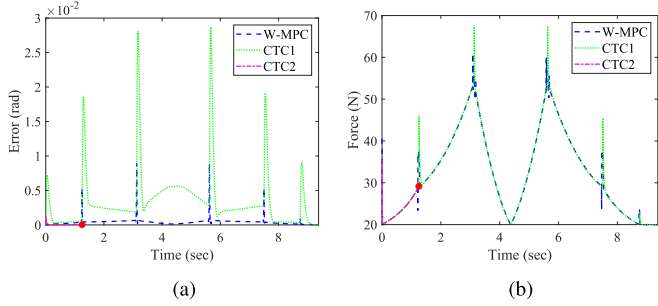


Fig. 11. Performance comparison: TR<sub>4</sub> nominal. (a) Tracking error norm. (b) Force vector norm.

more aggressive control actions

$$\text{CTC}_1 \text{ (low gain)} : K_p = 20^2 \times I_2, K_d = 20 \times I_2$$

$$\text{CTC}_2 \text{ (high gain)} : K_p = 90^2 \times I_2, K_d = 90 \times I_2.$$

**Nominal Case:** For the nominal case, the tracking performance comparison between W-MPC, CTC<sub>1</sub>, and CTC<sub>2</sub> is given in Figs. 10 and 11. For the smooth reference trajectory TR<sub>3</sub>, all the controllers successfully completed the tracking control with the W-MPC and high-gain CTC having a similarly good performance, while the low-gain CTC having a larger error. On the other hand, for the nonsmooth reference trajectory TR<sub>4</sub>, only W-MPC and low-gain CTC were able to complete the tracking task while the high-gain CTC failed due to the large tracking error caused by the discontinuity in the reference joint velocities. Similar to TR<sub>3</sub>, CTC<sub>1</sub> had a larger tracking error compared with the W-MPC in TR<sub>4</sub> tracking.

**Under External Disturbance:** In this scenario, the system was subject to a constant disturbance wrench  $\mathbf{w}_e = [1, -1]^T \text{ N}\cdot\text{m}$  that is unknown to the controller. The simulation results are shown in Figs. 12 and 13. Similar to the nominal case of TR<sub>3</sub>,

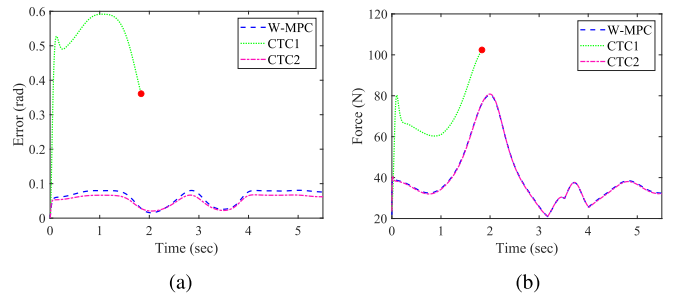


Fig. 12. Performance comparison: TR<sub>3</sub> under disturbance  $\mathbf{w}_e = [1, -1]^T \text{ N m}$ . (a) Tracking error norm. (b) Force vector norm.

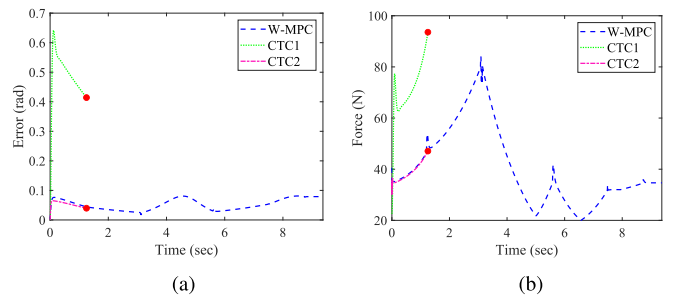


Fig. 13. Performance comparison: TR<sub>4</sub> under disturbance  $\mathbf{w}_e = [1, -1]^T \text{ N m}$ . (a) Tracking error norm. (b) Force vector norm.

Fig. 12(a) shows that both the W-MPC and CTC<sub>2</sub> completed the reference tracking under disturbance with a similar tracking performance while CTC<sub>1</sub> failed due to a weaker reference tracking capability from the smaller gains. As observed in Fig. 13(a), W-MPC was able to complete the tracking, while both CTC<sub>1</sub> and CTC<sub>2</sub> failed to track TR<sub>4</sub> with the former failing due to a weak tracking capability and the latter due to the reference discontinuity.

**Time Cost Comparison:** Consider the tracking control of TR<sub>3</sub> in nominal scenario using CTC<sub>1</sub> and W-MPC with different  $N$ ; the computational costs are summarized in Table III. As expected, the W-MPC had a higher computational cost compared with the CTC due to the larger optimization problem. Similarly, longer horizon in W-MPC would result in longer computational time. However, it can be observed that comparing with the CTC, the computational cost increase of the W-MPC with a short horizon  $N = 10$  is insignificant with respect to the control frequency (200 Hz).

In summary, the W-MPC achieved good tracking performance for both TR<sub>3</sub> and TR<sub>4</sub> without extensive parameter tuning in both nominal and non-nominal scenarios. In contrast, CTC would require careful gain tuning to suit different scenarios, where a low-gain CTC is better at adapting to trajectory non-smoothness while a high-gain CTC offers better robustness against model discrepancies. In the extreme case of nonsmooth trajectory TR<sub>4</sub> under external disturbances, CTC with both gains failed. On the other hand, the requirement for parameter-tuning in W-MPC is much lower. In fact, W-MPC successfully completed the tracking control under all the presented scenarios with a single set of parameters. Moreover, the online computational

load of W-MPC is suitable for real-time control with a shorter prediction horizon.

### B. Spatial CDR

The cable robot simulator (CRS) with six DoFs and eight cables, as modeled in [2], was simulated to show that the W-MPC can be applied to more general spatial CDRs. DFW was used as CRS' W-MPC workspace, which was defined by

$$\begin{aligned} |\dot{q}_{1,\dots,3}| &\leq 5 \text{ m/sec}, & |\dot{q}_{4,\dots,6}| &\leq 0.5 \text{ rad/sec} \\ |\ddot{q}_{1,\dots,3}| &\leq 14 \text{ m/sec}^2, & |\ddot{q}_{4,\dots,6}| &\leq 0.5 \text{ rad/sec}^2 \end{aligned}$$

$$10^3 \text{ N} \leq f_{1,\dots,8} \leq 1.4 \times 10^4 \text{ N}$$

where  $q_1$ ,  $q_2$ , and  $q_3$  represent three translational DoFs;  $q_4$ ,  $q_5$ , and  $q_6$  represent three rotational DoFs (Euler angles), and  $f_i$  represents the force of the  $i$ th cable in the system. Other control parameters for the W-MPC were

$$\tilde{\mathbf{Q}} = \text{diag}(\mathbf{I}_{6 \times 6}, \mathbf{0}_{6 \times 6}), \quad \tilde{\mathbf{R}} = 10^{-12} \times \mathbf{I}_{6 \times 6}, \quad \mathbf{H} = 10^{-11} \times \mathbf{I}_{8 \times 8}.$$

The prediction horizon was set as  $N = 10$  and the controller ran at 200 Hz without terminal constraint and cost. The trajectory was formed by a quintic interpolation of

$$\mathbf{q}_1 \xrightarrow[2 \text{ sec}]{} \mathbf{q}_2 \xrightarrow[2 \text{ sec}]{} \mathbf{q}_3 \xrightarrow[2 \text{ sec}]{} \mathbf{q}_3 \xrightarrow[2 \text{ sec}]{} \mathbf{q}_4 \xrightarrow[2 \text{ sec}]{} \mathbf{q}_1 \xrightarrow[2 \text{ sec}]{} \mathbf{q}_5 \quad (46)$$

where

$$\begin{aligned} \mathbf{q}_1 &= [6, 7.5, 4, 0, 0, 0]^\top, & \mathbf{q}_2 &= [5.5, 8, 3, 0.2, 0, 0]^\top \\ \mathbf{q}_3 &= [6, 7.5, 4, -0.2, 0.2, 0]^\top, & \mathbf{q}_4 &= [6.5, 7, 5, 0.2, 0.2, 0]^\top \\ \mathbf{q}_5 &= [6.5, 7, 5, 0, 0, 0]^\top. \end{aligned}$$

Furthermore, the following scenarios were considered:

- Scenario 1 (*nominal*): No model discrepancies.
- Scenario 2 (*disturbed*): An external disturbance wrench  $\mathbf{w}_e = [f_{ex}, f_{ey}, f_{ez}, \tau_{ex}, \tau_{ey}, \tau_{ez}]$  was applied, with  $f_{ex} = f_{ey} = 5000 \text{ N}$ ,  $f_{ez} = -10^4 \text{ N}$ , and  $\tau_{ex,ey,ez} = 500 \text{ N}\cdot\text{m}$ .
- Scenario 3 (*nonideal actuator*): A first-order system was considered to emulate the actuator's dynamics

$$\mathbf{f} = \mathbf{f}_{\text{prev}} + 0.2 (\mathbf{f}_{\text{cmd}} - \mathbf{f}_{\text{prev}}) \quad (47)$$

where  $\mathbf{f}_{\text{prev}}$ ,  $\mathbf{f}_{\text{cmd}}$ , and  $\mathbf{f}$  are the cable forces applied in the previous control cycle, the force commands, and the actual forces applied in the current control cycle, respectively.

The tracking control results are given in Fig. 14, showing that the proposed W-MPC can achieve good tracking performance in all the tested scenarios. Computation-wise, each control command generation took  $\sim 1.9 \text{ ms}$  in average, which satisfies the 200 Hz control frequency requirement.

## VI. HARDWARE VALIDATION

### A. Hardware Experiment Setup

As shown in Fig. 15, the constructed cable robot is composed of four cables and an end-effector that moves on the horizontal plane. The robot has three DoFs, represented by  $[x, y, \theta]^\top$ . In particular,  $x$  and  $y$  define the position of the end-effector

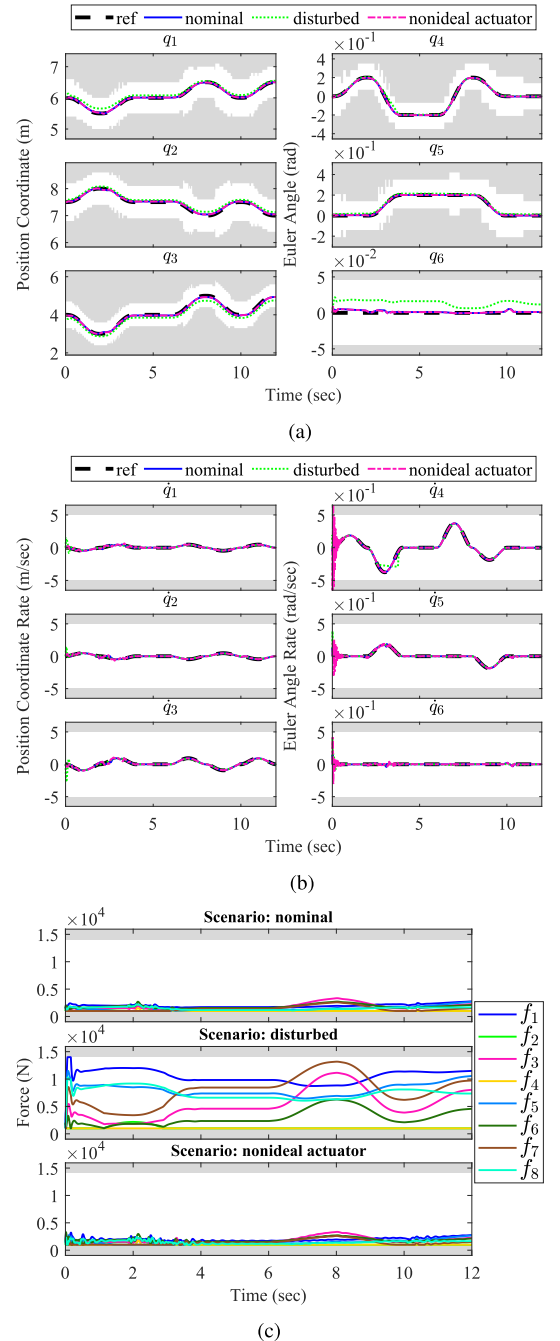


Fig. 14. Spatial CDR tracking under different scenarios. (a) Pose tracking. (b) Velocity tracking. (c) Cable forces.

within the horizontal plane and  $\theta$  represents the rotation of the end-effector along the normal direction of the horizontal plane. The cables were actuated by direct-drive motors (i.e., without gearbox) under the current control mode. For each motor, a linear relationship between the input current and the output cable force was calibrated and used to enable force control.

In terms of the control feedback, a forward kinematics (FK) module was used, which converted the cable length changes into a joint pose feedback. To validate the FK result, joint pose data was also collected from a motion tracker (NDI Polaris).

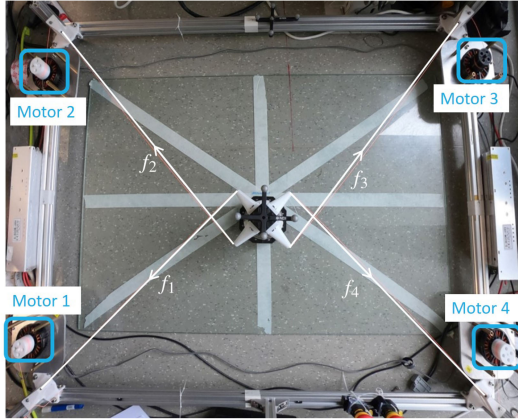


Fig. 15. PlanarXY cable-driven robot.

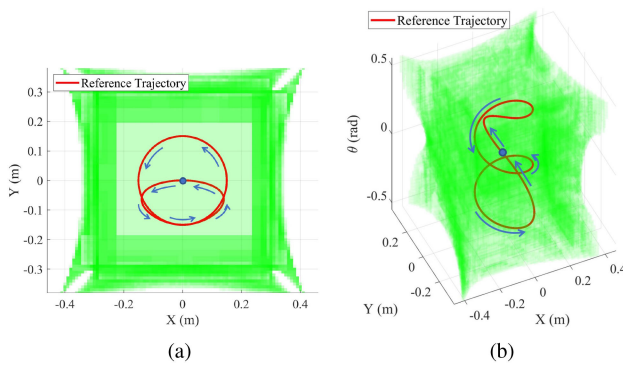


Fig. 16. DFW and TR6 reference trajectory of PlanarXY. (a) Top view. (b) 3-D view.

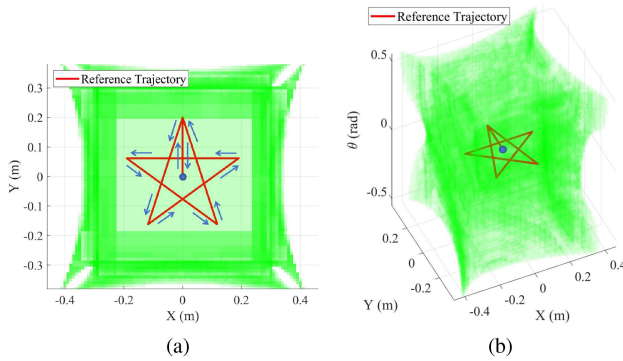


Fig. 17. DFW and TR7 reference trajectory of PlanarXY. (a) Top view. (b) 3-D view.

It should be noted that although the motion tracker data was collected through out the tracking task, it was *not* used in the control loop due to the low sampling rate of the former.

For the control task, two reference trajectories were defined, as shown in Figs. 16 and 17. In these figures, together with the reference trajectories, the DFW is also illustrated, as the green

shaded area, which were derived using the following constraints:

$$\begin{aligned} \dot{x}, \dot{y} &\in [-100, 100] \text{ m/s}, & \dot{\theta} &\in [-50, 50] \text{ rad/s} \\ \ddot{x}, \ddot{y} &\in [-4, 4] \text{ m/s}^2, & \ddot{\theta} &\in [-4, 4] \text{ rad/s}^2 \\ f_1, f_2, f_3, f_4 &\in [3, 35] \text{ N}. \end{aligned} \quad (48)$$

Using the DFW as the W-MPC workspace, the W-MPC can be formulated and applied to control the planar cable robot, with the control parameters set as follows:

$$\begin{aligned} \tilde{Q} &= \text{diag}(1, 1, 20, 10^{-8}, 10^{-8}, 2 \times 10^{-8}) \\ \tilde{R} &= 10^{-8} \cdot \text{diag}(1, 1, 0), H = 10^{-9} \times I_{4 \times 4}, N = 8. \end{aligned} \quad (49)$$

Each control command generation took  $\sim 0.86$  ms in average and a control frequency of 500 Hz was used in the experiment. Due to the large discrepancy between the mathematical model and the physical robot, terminal constraints and cost were not applied in this hardware experiment. In fact, as discussed in Sections VII-A and VII-B, the absence of terminal constraints and the use of a relatively short horizon ( $N = 8$ ) in this experiment allowed a tighter tracking, offering better robustness against model discrepancies.

### B. Hardware Validation Results and Discussions

The joint pose tracking results as well as the corresponding cable force commands are shown in Figs. 18 and 19, for TR6 and TR7, respectively. The unshaded areas in these result figures represent the allowed regions for joint poses, joint velocities and control inputs. In particular, the joint pose feasible regions were derived using the DFW corresponding to the allowed joint velocities, accelerations, and control inputs. As is shown in Figs. 18 and 19, all the constraints in W-MPC were strictly satisfied. It is worth noting that the joint feedback in the above result figures were computed using FK. In Fig. 20(a) and (d), the FK feedback, denoted as “X-FK,” “Y-FK,” and “ $\theta$ -FK,” the motion tracker feedback, denoted as “X-m,” “Y-m,” and “ $\theta$ -m,” together with the reference, denoted as “X-ref,” “Y-ref,” and “ $\theta$ -ref,” are given for TR6 and TR7, respectively. From the presented results, it can be concluded that the proposed W-MPC was able to provide good tracking performance on the prototype planar cable robot. The FK feedback and the motion tracker feedback also showed decent consistency, especially over the two translational DoFs.

## VII. DISCUSSIONS

### A. Role of Terminal Conditions

From Table II, it can be observed that when W-MPC is feasible with terminal conditions applied, the performance is similar to the case without terminal conditions. In addition, under non-nominal scenarios the feasibility of terminal constraints can only be achieved under long horizons. To understand this, it should be noted that the terminal constraints (Section III-D) assume a constant acceleration capability  $A_c$  for the terminal controller, which is also the assumed acceleration capability for any future steps over the prediction horizon. As a result, adding

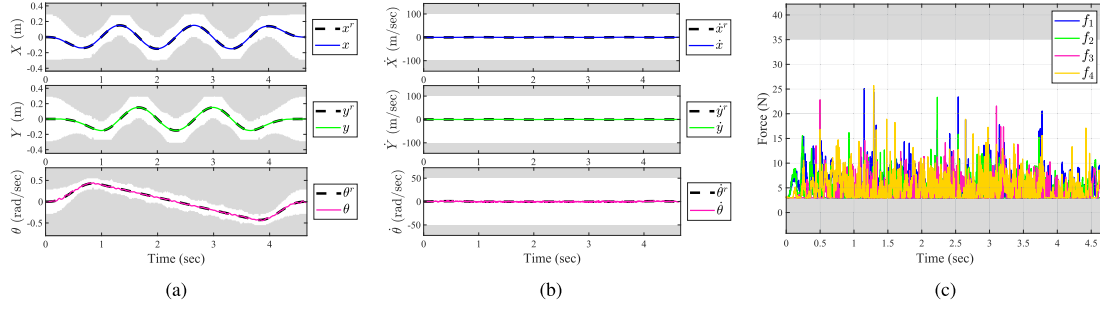


Fig. 18. TR6 tracking of Planar XY. (a) Joint pose tracking. (b) Joint velocity tracking. (c) Control input.

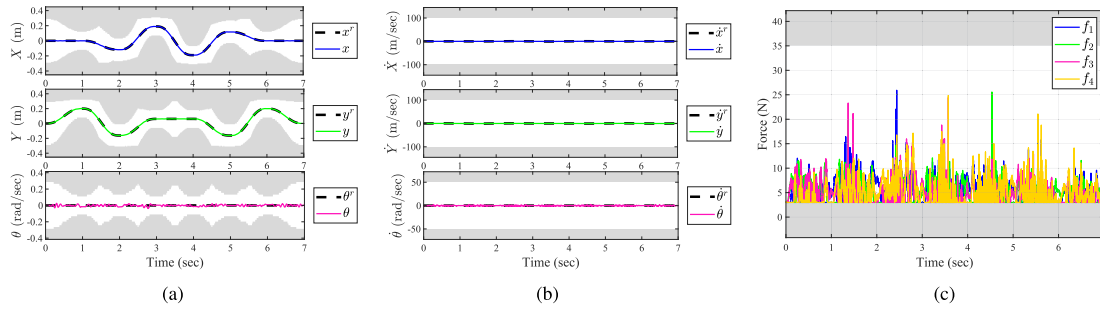


Fig. 19. TR7 tracking of Planar XY. (a) Joint pose tracking. (b) Joint velocity tracking. (c) Control input.

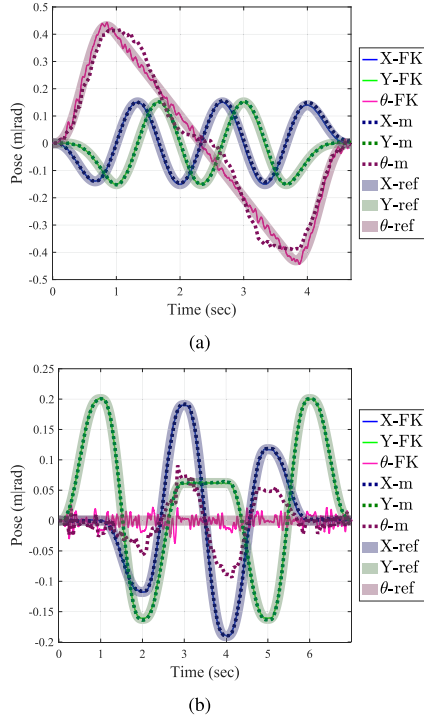


Fig. 20. Joint pose trajectories of Planar XY with external sensor. (a) TR6 pose trajectory. (b) TR7 pose trajectory.

terminal conditions with feasibility maintained is equivalent to running a long horizon W-MPC without terminal conditions. In this sense, despite the theoretical value, the terminal conditions shall be omitted in practical implementations of W-MPC, whose functionalities can be fully replaced by choosing a long horizon.

## B. Control Conservativeness

For a given reference tracking problem, W-MPC offers conservative solutions since it only uses a subset of the system's available control capability for the future time steps where only accelerations from a subset  $\mathcal{A}_c$  of the available acceleration set [56] are allowed to be used. On the other hand, since the first time step always uses the available acceleration set to confine the corresponding acceleration, it is not conservative. As a result, a conservativeness measure can be defined by  $(N - 1)/N$ , the ratio between the number of conservative time steps and the horizon length. In this sense, a smaller horizon length  $N$  will produce a less conservative solution with a smaller tracking error, which is consistent with observations from Table II. Combining this with Section VII-A, it can be concluded that  $N$  is a performance-sensitive parameter for W-MPC, which should be smaller for a tighter tracking and larger for safer and less aggressive control.

## C. Inherent Robustness

The nominal stability and recursive feasibility of W-MPC require Assumption 1 (in Appendix A) to hold. However, the violation of Assumption 1 is somehow inevitable in practice due to the model discrepancies and discrete control implementation, both causing small deviations between the actual and predicted state. Despite this, the simulation and hardware results showed that the W-MPC possesses *inherent robustness* such that these deviations deteriorate the performance but will not cause divergence or infeasibility, as long as the control frequency is sufficiently high (200 Hz for simulation and 500 Hz for hardware experiment).

#### D. Downsides of the Workspace-Based Convexification

While the use of workspace allows the convexification to be strictly feasible, it also comes with several drawbacks. First, as the reference gets closer to the boundary of the workspace, the design needs to be extra careful since the corresponding pose sets  $\mathcal{P}_i$  can be very small, resulting in a lower robustness, where infeasibility can happen even under very small model discrepancy. On the other hand, since the workspace corresponding to a smaller  $\mathcal{V}_c$  and  $\mathcal{A}_c$  is generally larger, this drawback inspires potential future works with the use of dynamically adjusted workspace, where the controller should switch to a workspace with smaller capability sets as it gets closer to the boundary of the original workspace. Second, the use of workspace requires an offline computation for each new reference trajectory, which can be computationally prohibitive for robots with higher DoFs due to the exponential computational complexity. Potential improvements can be achieved by investigating computational efficient workspace derivation/representation approaches, such as that in [57], [58].

### VIII. CONCLUSION

In this article, a W-MPC was proposed for the control of CDRs with nominal recursive feasibility and stability proven. The W-MPC scheme combines online control and offline workspace analysis with the computational load of the former mitigated by the latter. Through workspace analysis, a set of strictly feasible constraints of the system's joint pose, velocity, and acceleration were derived. These constraints allow the corresponding W-MPC optimization problem to be formulated into a quadratic program that can be efficiently solved. The control performance was demonstrated using simulations on a 2-link CDR and a spatial CDR, as well as hardware experiment on a 3-DoF planar CDR. Future works will focus on developing the W-MPC to be less conservative while maintaining its feasibility and stability.

### APPENDIX A

#### RECURSIVE FEASIBILITY AND STABILITY OF W-MPC

The nominal recursive feasibility and stability of MPC is a well-developed topic [44], [46], [59]. Using similar techniques, these properties are established in this section, which are specifically designed for W-MPC. In particular, the special terminal constraint/cost design from Section III-D is considered and the artificially introduced workspace-based constraints are explicitly accounted for.

#### A. Recursive Feasibility

Assume that the W-MPC can be feasibly solved at time step  $k - 1$ , then using the prediction from step  $k - 1$  with the terminal control law applied at the end of the horizon to extend the prediction, an initial guess can be given as follows to hot-start the W-MPC (26) for time step  $k$ :

$$\begin{aligned}\hat{\mathbf{X}}_k &= (\mathbf{x}_{k+1|k-1}, \dots, \mathbf{x}_{k+N-1|k-1}, \mathbf{x}_{k+N|k-1}) \\ \hat{\mathbf{V}}_k &= (\mathbf{v}_{k|k-1}, \dots, \mathbf{v}_{k+N-2|k-1}, \mathbf{v}_{k+N-1|k-1})\end{aligned}\quad (50)$$

where  $(\mathbf{x}_{k+1|k-1}, \dots, \mathbf{x}_{k+N-1|k-1})$  and  $(\mathbf{v}_{k|k-1}, \dots, \mathbf{v}_{k+N-2|k-1})$  are directly extracted from the previous prediction  $\mathbf{X}_{k-1}$  and  $\mathbf{V}_{k-1}$ , while  $\mathbf{v}_{k+N-1|k-1}$  and  $\mathbf{x}_{k+N|k-1}$  are extended virtual input and state using the terminal control law  $\kappa_i(\cdot)$  from (28)

$$\begin{aligned}\mathbf{v}_{k+N-1|k-1} &= \kappa_{k+N-1}(\mathbf{x}_{k+N-1|k-1}) \\ \mathbf{x}_{k+N|k-1} &= \mathbf{A}_d \mathbf{x}_{k+N-1|k-1} + \mathbf{B}_d \kappa_{k+N-1}(\mathbf{x}_{k+N-1|k-1}).\end{aligned}$$

Following Assumption 1 for the nominal case, Theorem 2 shows that for time step  $k$ , the initial guess from (50) is strictly feasible, guaranteeing the nominal recursive feasibility.

*Assumption 1 (Nominal Case Assumption):* In nominal case, the actual and predicted states are identical. Denote the actual state and the predicted virtual input at time step  $k - 1$  as  $\mathbf{x}_{k-1}$  and  $\mathbf{v}_{k-1|k-1}$ , respectively, the subsequent state prediction can be given as

$$\mathbf{x}_{k|k-1} = \mathbf{A}_d \mathbf{x}_{k-1} + \mathbf{B}_d \mathbf{v}_{k-1|k-1}.$$

Then, the actual executed virtual input and the subsequent state are as predicted, i.e.,  $\mathbf{v}_{k-1} = \mathbf{v}_{k-1|k-1}$  and  $\mathbf{x}_k = \mathbf{x}_{k|k-1}$ .

*Theorem 2 (Nominal Recursive Feasibility):* Without loss of generality, consider the solution state horizon and virtual input horizon of the W-MPC (26) at time step  $k - 1$  as

$$\begin{aligned}\mathbf{X}_{k-1} &= (\mathbf{x}_{k-1}, \mathbf{x}_{k|k-1}, \dots, \mathbf{x}_{k+N-1|k-1}) \\ \mathbf{V}_{k-1} &= (\mathbf{v}_{k-1|k-1}, \mathbf{v}_{k|k-1}, \dots, \mathbf{v}_{k+N-2|k-1}).\end{aligned}\quad (51)$$

For the nominal case, an initial guess  $(\hat{\mathbf{X}}_k, \hat{\mathbf{V}}_k, \hat{\mathbf{f}}_k)$  can be derived for step  $k$  based on previous predictions (51) and terminal control law (28) to strictly satisfy all of the constraints

$$\mathbf{M}_k \mathbf{v}_{k|k-1} + \mathbf{c}_k + \mathbf{g}_k = -\mathbf{L}_k^T \hat{\mathbf{f}}_k, \hat{\mathbf{f}}_k \in \mathcal{F} \quad (52a)$$

$$\hat{\mathbf{X}}_k = \mathbf{A} \mathbf{x}_k + \mathbf{B} \hat{\mathbf{V}}_k \quad (52b)$$

$$\hat{\mathbf{X}}_k \in \mathcal{P}_{k+1} \times \mathcal{V}_c \times \dots \times \mathcal{P}_{k+N-1} \times \mathcal{V}_c \times \phi_{k+N} \quad (52c)$$

$$\hat{\mathbf{V}}_k \in \mathbb{R}^n \times \mathcal{A}_c^{N-1}. \quad (52d)$$

*Proof:* Since (51) is a feasible solution of time step  $k - 1$ , the following is satisfied:

$$\mathbf{x}_{k-1} = \mathbf{A} \mathbf{x}_{k-1} + \mathbf{B} \mathbf{V}_{k-1}$$

Then, for the terminal virtual control input  $\mathbf{v}_{k+N-1|k-1} = \kappa_{k+N-1}(\mathbf{x}_{k+N-1|k-1})$ , the predicted state is formulated as

$$\mathbf{x}_{k+N|k-1} = \mathbf{A}_d \mathbf{x}_{k+N-1|k-1} + \mathbf{B}_d \mathbf{v}_{k+N-1|k-1}.$$

Hence, the relationship between  $\hat{\mathbf{X}}_k$  and  $\hat{\mathbf{V}}_k$  from (50) can be given as

$$\hat{\mathbf{X}}_k = \mathbf{A} \mathbf{x}_{k|k-1} + \mathbf{B} \hat{\mathbf{V}}_k$$

where  $\mathbf{x}_{k|k-1} = \mathbf{A}_d \mathbf{x}_{k-1} + \mathbf{B}_d \mathbf{v}_{k-1|k-1}$  is the predicted state for time step  $k$ . Following Assumption 1,  $\mathbf{x}_k = \mathbf{x}_{k|k-1}$  in nominal case; hence, constraint (52b) is satisfied. Additionally, as a feasible solution to (26),  $\mathbf{X}_{k-1}$  and  $\mathbf{V}_{k-1}$  in (51) also satisfy

$$\mathbf{X}_{k-1} \in \mathcal{P}_k \times \mathcal{V}_c \times \dots \times \mathcal{P}_{k+N-2} \times \mathcal{V}_c \times \phi_{k+N-1}$$

$$\mathbf{V}_{k-1} \in \mathcal{A}_{k-1} \times \mathcal{A}_c^{N-1}.$$

Since  $\mathbf{x}_{k+N-1|k-1} \in \phi_{k+N-1}$  holds, according to Lemma 1, the virtual input  $\mathbf{v}_{k+N-1|k-1}$  and subsequent state  $\mathbf{x}_{k+N|k-1}$  satisfy

$$\begin{aligned}\mathbf{x}_{k+N|k-1} &\in \phi_{k+N} \\ \mathbf{v}_{k+N-1|k-1} &\in \mathcal{A}_c.\end{aligned}$$

Consequently, (50) satisfies the following constraint:

$$\begin{aligned}\hat{\mathbf{X}}_k &\in \mathcal{P}_{k+1} \times \mathcal{V}_c \times \cdots \times \mathcal{P}_{k+N-2} \times \mathcal{V}_c \times \phi_{k+N-1} \times \phi_{k+N} \\ \hat{\mathbf{V}}_k &\in \mathcal{A}_c^N.\end{aligned}\quad (53)$$

Since  $\forall i > 0$ , the terminal sets  $\phi_i$  are designed such that  $\phi_i \subset \mathcal{P}_i \times \mathcal{V}_c$ , while the virtual input set  $\mathcal{A}_c$  satisfies  $\mathcal{A}_c \subset \mathcal{A}(\mathbf{x})$ ,  $\forall \mathbf{x} \in \mathcal{P}_i \times \mathcal{V}_c$ , constraints (52c) and (52d) are satisfied.

Additionally, since  $\mathbf{x}_k = \mathbf{x}_{k|k-1} \in \mathcal{P}_k \times \mathcal{V}_c$ , the virtual input constraint  $\mathbf{v}_{k|k-1} \in \mathcal{A}_c \subset \mathcal{A}_k$  can be derived. Then, according to (15), there exists a cable force vector  $\hat{\mathbf{f}}_k$  satisfying the EoM and cable force constraints (52a). As such,  $(\hat{\mathbf{X}}_k, \hat{\mathbf{V}}_k, \hat{\mathbf{f}}_k)$  satisfies constraints (52), and hence can be used as a feasible initial guess for (26) at time step  $k$ , satisfying *recursive feasibility*. ■

### B. Stability

The following definitions and propositions will be used to show the proposed W-MPC's nominal case (Assumption 1) stability. Propositions 1 and 2 can be easily proven using Definitions 3 and 4 while Proposition 3 is based on Definition 4 as well as the feasibility of the reference trajectory.

**Definition 3 (Estimated Cost):** The estimated optimization cost for the W-MPC at time step  $k$  using the predictions from the previous time step ( $\mathbf{x}_{k|k-1}$ ,  $\hat{\mathbf{X}}_k$  and  $\hat{\mathbf{V}}_k$ ) can be defined as

$$\hat{J}_k = \hat{\eta}_k + \|\hat{\mathbf{f}}_k\|_H^2$$

where

$$\begin{aligned}\hat{\eta}_k &= \|\mathbf{x}_{k|k-1} - \mathbf{x}_k^r\|_Q^2 + \|\mathbf{A}\mathbf{x}_{k|k-1} + \mathbf{B}\hat{\mathbf{V}}_k - \mathbf{X}_k^r\|_Q^2 \\ &\quad + \|\hat{\mathbf{V}}_k - \mathbf{V}_k^r\|_R^2\end{aligned}$$

and  $\hat{\mathbf{f}}_k$  is a feasible cable force vector corresponding to the predicted virtual input  $\mathbf{v}_{k|k-1}$ .

**Definition 4 (Optimized Cost):** The optimized cost for the W-MPC at time step  $k$  can be defined as

$$J_k = \eta_k + \|\mathbf{f}_k\|_H^2$$

where

$$\eta_k = \|\mathbf{x}_k - \mathbf{x}_k^r\|_Q^2 + \|\mathbf{A}\mathbf{x}_k + \mathbf{B}\mathbf{V}_k - \mathbf{X}_k^r\|_Q^2 + \|\mathbf{V}_k - \mathbf{V}_k^r\|_R^2$$

and  $\mathbf{X}_k$ ,  $\mathbf{V}_k$ , and  $\mathbf{f}_k$  can be determined by solving (26) with  $\mathbf{x}_k$ .

**Proposition 1:** The relationship between  $\eta_{k-1}$  and  $\hat{\eta}_k$  is

$$\eta_{k-1} = \hat{\eta}_k + l_{k-1}$$

$$\text{with } l_{k-1} = \|\mathbf{x}_{k-1} - \mathbf{x}_{k-1}^r\|_Q^2 + \|\mathbf{v}_{k-1|k-1} - \mathbf{v}_{k-1}^r\|_R^2.$$

**Proposition 2:** From Theorem 2,  $(\hat{\mathbf{X}}_k, \hat{\mathbf{V}}_k, \hat{\mathbf{f}}_k)$  can be used as a feasible initial guess to solve (26). As a result, the optimized

cost  $J_k$  will be no larger than the initial guess cost  $\hat{J}_k$

$$J_k - \hat{J}_k = \eta_k - \hat{\eta}_k + \|\mathbf{f}_k\|_H^2 - \|\hat{\mathbf{f}}_k\|_H^2 \leq 0.$$

**Proposition 3 (W-MPC Lyapunov Candidate Function):** For time step  $k$ , a Lyapunov candidate function can be defined as

$$\eta_k = \|\mathbf{x}_k - \mathbf{x}_k^r\|_Q^2 + \|\mathbf{A}\mathbf{x}_k + \mathbf{B}\mathbf{V}_k - \mathbf{X}_k^r\|_Q^2 + \|\mathbf{V}_k - \mathbf{V}_k^r\|_R^2$$

guaranteeing that

$$\eta_k = 0 \iff l_k = 0 \iff \mathbf{x}_k = \mathbf{x}_k^r.$$

**Lemma 2 (Nominal Asymptotic Stability):** The W-MPC is asymptotically stable under nominal conditions (Assumption 1) if all the singular values of  $H$  in (26) are zero.

*Proof:* If all the singular values of  $H$  are zero,  $\|\mathbf{f}_k\|_H^2 = \|\hat{\mathbf{f}}_k\|_H^2 = 0$ . Hence, substitution of Proposition 1 into Proposition 2 results in the relationship  $\eta_k - \eta_{k-1} \leq -l_{k-1}$ . Then, following Proposition 3,  $\eta_k - \eta_{k-1} = 0$  for  $\eta_{k-1} = 0$  and  $\eta_k - \eta_{k-1} < 0$  if  $\eta_{k-1} > 0$ . As such, the system is asymptotically stable. ■

Lemma 2 shows that the proposed W-MPC is asymptotically stable if the minimization of cable forces is not considered. In practice, considering the actuation redundancy that usually exists in CDRs, it is desirable to consider the cable force minimization to avoid excessive cable tension. However, the consideration of cable forces will affect asymptotic stability as minimizing the cable forces may be in conflict with tracking performance. As shown in Theorem 3, the minimization of cable forces in the W-MPC results in bounded stability.

**Theorem 3 (Nominal Bounded Stability):** The W-MPC is ultimately bounded stable under nominal conditions (Assumption 1) if  $H$  has a finite maximum singular value.

*Proof:* Considering the cable force constraint  $\mathbf{f} \in \mathcal{F}$ , all the feasible cable forces are bounded by

$$\forall \mathbf{f} \in \mathcal{F} : f_{\min} \leq \|\mathbf{f}\|^2 \leq f_{\max}$$

with  $f_{\max} > f_{\min} \geq 0$ . Denote the maximum singular value of  $H$  as  $\sigma > 0$ , the following bound can then be derived:

$$\forall \hat{\mathbf{f}}_k, \mathbf{f}_k \in \mathcal{F} : \left| \|\mathbf{f}_k\|_H^2 - \|\hat{\mathbf{f}}_k\|_H^2 \right| \leq \sigma f_{\max}.$$

Consequently from Proposition 2,  $\eta_k - \eta_{k-1} \leq \sigma f_{\max} - l_{k-1}$ , which further gives  $\eta_k - \eta_{k-1} < 0$  if  $l_{k-1} > \sigma f_{\max}$ . In other words, the Lyapunov function  $\eta_{k-1}$  will decrease as long as  $l_{k-1} > \sigma f_{\max}$ . On the other hand, by definition  $l_{k-1} \leq \eta_{k-1}$ , hence  $l_{k-1}$  will decrease as  $\eta_{k-1}$  does until  $l_{k-1} \leq \sigma f_{\max}$ . Since the above results hold for any time step  $k$  with the state error bounded by  $\|\mathbf{x}_k - \mathbf{x}_k^r\|_Q^2 \leq l_k$ , it can be concluded that the state tracking error will eventually be bounded by set

$$\Omega_\sigma = \left\{ \mathbf{x}_k - \mathbf{x}_k^r \in \mathbb{R}^{2n} \mid \|\mathbf{x}_k - \mathbf{x}_k^r\|_Q^2 \leq \sigma f_{\max} \right\}. \quad (54)$$

This shows the ultimate bounded stability of W-MPC. ■

**Corollary 1:** The ultimate state tracking error bound (54) can be arbitrarily small by designing the weight matrix  $H$  with a small enough maximum singular value  $\sigma$

$$\lim_{\sigma \rightarrow 0} \Omega_\sigma = \{\mathbf{0}\}.$$

## REFERENCES

- [1] H. Li, J. Sun, G. Pan, and Q. Yang, "Preliminary running and performance test of the huge cable robot of FAST telescope," in *Mechanisms and Machine Science*. Berlin, Germany: Springer International Publishing, 2018, pp. 402–414.
- [2] P. Miermeister *et al.*, "The cable robot simulator large scale motion platform based on cable robot technology," in *Proc. IEEE/RSJ Int. Conf. Intell. Robot. Syst.*, Oct.–Nov. 2016, pp. 3024–3029.
- [3] J. Albus, R. Bostelman, and N. Dagalakis, "The NIST SPIDER, A robot crane," *J. Res. Natl. Inst. Standards Technol.*, vol. 97, no. 3, pp. 373–385, May 1992.
- [4] Y. Wu, H. H. Cheng, A. Fingrut, K. Crolla, Y. Yam, and D. Lau, "CU-brick cable-driven robot for automated construction of complex brick structures: From simulation to hardware realisation," in *Proc. IEEE Int. Conf. Simul. Model. Program. Auton. Robot.*, 2018, pp. 166–173.
- [5] R. Dekker, A. K. Jepour, and S. Behzadipour, "Design and testing of an ultra-high-speed cable robot," *Int. J. Robot. Autom.*, vol. 21, no. 1, pp. 25–34, 2006.
- [6] R. Buckingham and A. Graham, "Nuclear snake-arm robots," *Ind. Robot. An. Int. J.*, vol. 39, no. 1, pp. 6–11, Jan. 2012.
- [7] Y. Asano *et al.*, "Human mimetic musculoskeletal humanoid Kengoro toward real world physically interactive actions," in *Proc. IEEE-RAS 16th Int. Conf. Humanoid Robot.*, Nov. 2016, pp. 876–883.
- [8] Y. Mao and S. K. Agrawal, "Design of a cable-driven arm exoskeleton (CAREX) for neural rehabilitation," *IEEE Trans. Robot.*, vol. 28, no. 4, pp. 922–931, Aug. 2012.
- [9] D. Lau, J. Eden, S. K. Halgamuge, and D. Oetomo, "Cable function analysis for the musculoskeletal static workspace of a human shoulder," *Mech. Mach. Sci.*, vol. 32, pp. 263–274, Dec. 2015.
- [10] D. Lau, J. Eden, D. Oetomo, and S. K. Halgamuge, "Musculoskeletal static workspace analysis of the human shoulder as a cable-driven robot," *IEEE/ASME Trans. Mechatronics*, vol. 20, no. 2, pp. 978–984, Apr. 2015.
- [11] R. Kurtz and V. Hayward, "Dexterity measures with unilateral actuation constraints: The n+1 case," *Adv. Robot.*, vol. 9, no. 5, pp. 561–577, Jan. 1994.
- [12] T. Dallej, M. Gouttefarde, N. Andreff, M. Michelin, and P. Martinet, "Towards vision-based control of cable-driven parallel robots," in *Proc. IEEE/RSJ Int. Conf. Intell. Robot. Syst.*, 2011, pp. 2855–2860.
- [13] T. Dallej, M. Gouttefarde, N. Andreff, P.-E. Hervé, and P. Martinet, "Modeling and vision-based control of large-dimension cable-driven parallel robots using a multiple-camera setup," *Mechatronics*, vol. 61, pp. 20–36, Aug. 2019.
- [14] R. Babaghasabha, M. A. Khosravi, and H. D. Taghirad, "Adaptive robust control of fully-constrained cable driven parallel robots," *Mechatronics*, vol. 25, no. 2, pp. 27–36, Feb. 2015.
- [15] M. A. Khosravi and H. D. Taghirad, "Robust PID control of fully-constrained cable driven parallel robots," *Mechatronics*, vol. 24, no. 2, pp. 87–97, Mar. 2014.
- [16] S.-R. Oh, J.-C. Ryu, and S. K. Agrawal, "Dynamics and control of a helicopter carrying a payload using a cable-suspended robot," *J. Mech. Des.*, vol. 128, no. 5, 2006, Art. no. 1113.
- [17] S. R. Oh and S. K. Agrawal, "Cable suspended planar robots with redundant cables: Controllers with positive tensions," *IEEE Trans. Robot.*, vol. 21, no. 3, pp. 457–465, Jun. 2005.
- [18] M. Hassan and A. Khajepour, "Optimization of actuator forces in cable-based parallel manipulators using convex analysis," *IEEE Trans. Robot.*, vol. 24, no. 3, pp. 736–740, Jun. 2008.
- [19] H. D. Taghirad and Y. B. Bedoustanti, "An analytic-iterative redundancy resolution scheme for cable-driven redundant parallel manipulators," *IEEE Trans. Robot.*, vol. 27, no. 6, pp. 1137–1143, Dec. 2011.
- [20] S. Abdolshah and G. Rosati, "First experimental testing of a dynamic minimum tension control (DMTC) for cable driven parallel robots," *Mech. Mach. Sci.*, vol. 32, pp. 239–248, 2015.
- [21] A. Alp and S. Agrawal, "Cable suspended robots: Design, planning and control," in *Proc. IEEE Int. Conf. Robot. Autom.*, Jun. 2002, vol. 4, pp. 4275–4280.
- [22] A. Bemporad, "Reference governor for constrained nonlinear systems," *IEEE Trans. Automat. Control*, vol. 43, no. 3, pp. 415–419, Mar. 1998.
- [23] E. Gilbert and I. Kolmanovsky, "Nonlinear tracking control in the presence of state and control constraints: A generalized reference governor," *Automatica*, vol. 38, no. 12, pp. 2063–2073, Dec. 2002.
- [24] S. R. Oh and S. K. Agrawal, "A reference governor-based controller for a cable robot under input constraints," *IEEE Trans. Control Syst. Technol.*, vol. 13, no. 4, pp. 639–645, Jul. 2005.
- [25] S. R. Oh and S. K. Agrawal, "Generation of feasible set points and control of a cable robot," *IEEE Trans. Robot.*, vol. 22, no. 3, pp. 551–558, Jun. 2006.
- [26] M. Katliar, J. Fischer, G. Frison, M. Diehl, H. Teufel, and H. H. Bülfhoff, "Nonlinear model predictive control of a cable-robot-based motion simulator," *IFAC-PapersOnLine*, vol. 50, no. 1, pp. 9833–9839, Jul. 2017.
- [27] A. Ghasemi, "Application of linear model predictive control and input-output linearization to constrained control of 3D cable robots," *Modern Mech. Eng.*, vol. 1, no. 2, pp. 69–76, 2011.
- [28] J. C. Santos, A. Chemori, and M. Gouttefarde, "Model predictive control of large-dimension cable-driven parallel robots," in *Mechanisms and Machine Science*. The Netherlands: Springer, Jun. 2019, vol. 74, pp. 221–232.
- [29] J. C. Santos, A. Chemori, and M. Gouttefarde, "Redundancy resolution integrated model predictive control of CDPRs: Concept, implementation and experiments," in *Proc. IEEE Int. Conf. Robot. Autom.*, May 2020, pp. 3889–3895.
- [30] S. Gros, M. Zanon, R. Quirynen, A. Bemporad, and M. Diehl, "From linear to nonlinear MPC: Bridging the gap via the real-time iteration," *Int. J. Control.*, vol. 93, no. 1, pp. 62–80, Sep. 2020.
- [31] B. Houska, H. J. Ferreau, and M. Diehl, "An auto-generated real-time iteration algorithm for nonlinear MPC in the microsecond range," *Automatica*, vol. 47, no. 10, pp. 2279–2285, Oct. 2011.
- [32] L. T. Biegler, "Efficient solution of dynamic optimization and NMPC problems," in *Nonlinear Model Predictive Control*, F. Allgöwer and A. Zheng, Eds. Basel: Birkhäuser Basel, 2000, vol. 26, pp. 219–243.
- [33] M. Diehl, H. G. Bock, J. P. Schlöder, R. Findeisen, Z. Nagy, and F. Allgöwer, "Real-time optimization and nonlinear model predictive control of processes governed by differential-algebraic equations," *J. Process Control*, vol. 12, no. 4, pp. 577–585, Jun. 2002.
- [34] J. Levine, "Static and dynamic state feedback linearization," in *Nonlinear System*. Boston, MA, USA: Springer, 1997, pp. 93–126.
- [35] W. R. van Soest, Q. P. Chu, and J. a. Mulder, "Combined feedback linearization and constrained model predictive control for entry flight," *J. Guid. Control Dyn.*, vol. 29, no. 2, pp. 427–434, Mar. 2006.
- [36] F. Schnelle and P. Eberhard, "Constraint mapping in a feedback linearization/MPC scheme for trajectory tracking of underactuated multi-body systems," *IFAC-PapersOnLine*, vol. 48, no. 23, pp. 446–451, 2015.
- [37] D. Simon, J. Lofberg, and T. Glad, "Nonlinear model predictive control using feedback linearization and local inner convex constraint approximations," in *Proc. Eur. Control Conf.*, 2013, pp. 2056–2061.
- [38] Y. V. Pant, H. Abbas, and R. Mangharam, "Robust model predictive control for non-linear systems with input and state constraints via feedback linearization," in *Proc. IEEE 55th Conf. Decis. Control*, Dec. 2016, pp. 5694–5699.
- [39] D. Lau, J. Eden, Y. Tan, and D. Oetomo, "CASPR: A comprehensive cable-robot analysis and simulation platform for the research of cable-driven parallel robots," in *Proc. IEEE/RSJ Int. Conf. Intell. Robot. Syst.*, vol. 2016, Oct.–Nov. 2016, pp. 3004–3011.
- [40] Z. Zhang, H. H. Cheng, and D. Lau, "Efficient wrench-closure and interference free conditions verification for cable-driven parallel robot trajectories using a ray-based method," *IEEE Robot. Autom. Lett.*, vol. 5, no. 1, pp. 8–15, Jan. 2020.
- [41] D. Lau, D. Oetomo, and S. K. Halgamuge, "Generalized modeling of multilink cable-driven manipulators with arbitrary routing using the cable-routing matrix," *IEEE Trans. Robot.*, vol. 29, no. 5, pp. 1102–1113, Oct. 2013.
- [42] J. M. Bravo, T. Alamo, and E. F. Camacho, "Robust MPC of constrained discrete-time nonlinear systems based on approximated reachable sets," *Automatica*, vol. 42, no. 10, pp. 1745–1751, Oct. 2006.
- [43] E. Todorov, "Optimal control theory," in *Bayesian Brain*. Cambridge, MA, USA: MIT Press, Dec. 2006, pp. 268–298.
- [44] D. Mayne, J. Rawlings, C. Rao, and P. Scokaert, "Constrained model predictive control: Stability and optimality," *Automatica*, vol. 36, no. 6, pp. 789–814, Jun. 2000.
- [45] J. B. Rawlings and D. Q. Mayne, *Model Predictive Control: Theory and Design*, 2nd ed. Madison, WI, USA: Nob Hill Publishing, 2009.
- [46] D. Mayne, "An apologia for stabilising terminal conditions in model predictive control," *Int. J. Control.*, vol. 86, no. 11, pp. 2090–2095, Nov. 2013.
- [47] S. Lessanibahri, M. Gouttefarde, S. Caro, and P. Cardou, "Twist feasibility analysis of cable-driven parallel robots," in *Cable-Driven Parallel Robots*, C. Gosselin, P. Cardou, T. Bruckmann, and A. Pott, Eds. Cham, Switzerland: Springer International Publishing, 2018, pp. 128–139.

- [48] S. Bouchard, C. Gosselin, and B. Moore, “On the ability of a cable-driven robot to generate a prescribed set of wrenches,” *J. Mech. Robot.*, vol. 2, no. 1, pp. 1–10, May 2010.
- [49] M. Gouttefarde and S. Krut, “Characterization of parallel manipulator available wrench set facets,” *Adv. Robot Kinemat. Motion Man Mach.*, vol. 4, pp. 475–482, 2010.
- [50] L. Sciavicco and B. Siciliano, *Modelling and Control of Robot Manipulators*, 2nd ed. Berlin, Germany: Springer, 2001.
- [51] U. Naumann, “PAMM: Proceedings in applied mathematics and mechanics,” *Proc. Appl. Math. Mechanics*, vol. 7, no. 1, pp. 1140205–1140206, 2007. [Online.] Available: <https://onlinelibrary.wiley.com/journal/16177061>
- [52] R. Featherstone, *Rigid Body Dynamics Algorithms*. Boston, MA, USA: Springer, 2008.
- [53] Y. Zhang and L. Gao, “On numerical solution of the maximum volume ellipsoid problem,” *SIAM J. Optim.*, vol. 14, no. 1, pp. 53–76, Jan. 2003.
- [54] H. J. Ferreau, C. Kirches, A. Potschka, H. G. Bock, and M. Diehl, “qpOASES: A parametric active-set algorithm for quadratic programming,” *Math. Program. Comput.*, vol. 6, no. 4, pp. 327–363, Dec. 2014.
- [55] J.-J. E. Slotine and W. Li, “On the adaptive control of robot manipulators,” *Int. J. Rob. Res.*, vol. 6, no. 3, pp. 49–59, Sep. 1987.
- [56] J. Eden, D. Lau, Y. Tan, and D. Oetomo, “Available acceleration set for the study of motion capabilities for cable-driven robots,” *Mech. Mach. Theory*, vol. 105, pp. 320–336, Nov. 2016.
- [57] A. Pott, “Efficient computation of the workspace boundary, its properties and derivatives for cable-driven parallel robots,” in *Mechanisms and Machine Science*. Cham, Switzerland: Springer, 2018, vol. 50, pp. 190–197.
- [58] G. Abbasnejad, J. Eden, and D. Lau, “Generalized ray-based lattice generation and graph representation of wrench-closure workspace for arbitrary cable-driven robots,” *IEEE Trans. Robot.*, vol. 35, no. 1, pp. 147–161, Feb. 2019.
- [59] P. Scokaert, D. Mayne, and J. Rawlings, “Suboptimal model predictive control (feasibility implies stability),” *IEEE Trans. Automat. Control*, vol. 44, no. 3, pp. 648–654, Mar. 1999.



**Chen Song** received the B.Eng. and M.Eng. degrees in aerospace engineering from Northwestern Polytechnical University, Xi'an, China, in 2013 and 2016, respectively, and the Ph.D. degree in robotics from the Chinese University of Hong Kong, Hong Kong, China, in 2021.

He is currently a Systems Analyst with Cornerstone Robotics, Hong Kong. His research interests include optimization-based control, analysis and control of robotic systems subject to constraints and/or actuation redundancy, and cable-driven mechanisms.



**Darwin Lau** (Senior Member, IEEE) received the B.Eng. (Hons) degree in mechatronics, B.CS. degree, and the Ph.D. degree in mechanical engineering and robotics from the University of Melbourne, Parkville, VIC, Australia, in 2008 and 2014, respectively.

He was a Postdoctoral Research Fellow with Pierre and Marie Curie University from 2014 to 2015. He is currently an Associate Professor with the Department of Mechanical and Automation Engineering, Chinese University of Hong Kong, Hong Kong. His research interests include kinematics, dynamics and control of redundantly actuated mechanisms, cable-driven parallel manipulators, construction and architectural robotics, and bioinspired robots.